NAVAL POSTGRADUATE SCHOOL

MONTEREY, CALIFORNIA

THESIS

FRICTION STIR PROCESSING PARAMETERS AND PROPERTY DISTRIBUTIONS IN CAST NICKEL ALUMINUM BRONZE

by

Brian P. Rosemark

December 2006

Thesis Advisor:	Terry R. McNelley
Co-Advisor:	Srinivasan Swaminathan

Approved for public release; distribution is unlimited

THIS PAGE INTENTIONALLY LEFT BLANK

REPORT DOCUMENTATION PAGE			Form Approved OMB No. 0704-0188
Public reporting burden for this collection of information is estimated to average 1 hour per response, including the time for reviewing instruction, searching existing data sources, gathering and maintaining the data needed, and completing and reviewing the collection of information. Send comments regarding this burden estimate or any other aspect of this collection of information, including suggestions for reducing this burden, to Washington headquarters Services, Directorate for Information Operations and Reports, 1215 Jefferson Davis Highway, Suite 1204, Arlington, VA 22202-4302, and to the Office of Management and Budget, Paperwork Reduction Project (0704-0188) Washington DC 20503.			
1. AGENCY USE ONLY ***(Leave blank)***	**2. REPORT DATE** December 2006	**3. REPORT TYPE AND DATES COVERED** Master's Thesis	
4. TITLE AND SUBTITLE Friction Stir Processing Parameters and Property Distributions in Cast Nickel Aluminum Bronze		**5. FUNDING NUMBERS**	
6. AUTHOR(S) Brian P. Rosemark			
7. PERFORMING ORGANIZATION NAME(S) AND ADDRESS(ES) Naval Postgraduate School Monterey, CA 93943-5000		**8. PERFORMING ORGANIZATION REPORT NUMBER**	
9. SPONSORING /MONITORING AGENCY NAME(S) AND ADDRESS(ES) N/A		**10. SPONSORING/MONITORING AGENCY REPORT NUMBER**	
11. SUPPLEMENTARY NOTES The views expressed in this thesis are those of the author and do not reflect the official policy or position of the Department of Defense or the U.S. Government.			
12a. DISTRIBUTION / AVAILABILITY STATEMENT Approved for public release; distribution is unlimited.		**12b. DISTRIBUTION CODE** A	

13. ABSTRACT (maximum 200 words)

Cast nickel-aluminum bronze (NAB) alloy is specified for many marine applications, including ship propellers, due to its excellent corrosion-resistance combined with acceptable mechanical properties. Friction stir processing (FSP) can be used to improve the alloy's mechanical properties by localized microstructure modification in the cast material. FSP converts an as-cast microstructure to a wrought condition in the absence of macroscopic shape change, closes porosity, and provides a means to surface harden the castings. The closure of porosity near the surface of the material may shorten the manufacturing and processing time for ship propellers. The surface hardening of cast NAB alloy can be used to increase the wear life of ship propellers. Rockwell Scientific Corporation (now Teledyne Scientific Corporation) supplied three Nickel Aluminum Bronze alloy plates which have been friction stir processed in a raster pattern under a Defense Advanced Research Project Agency (DARPA) project. Each plate had been processed using a different tool RPM and IPM (inches per minute of transverse) combination. Miniature tensile samples were sectioned from the FSP zone and surrounding base metal and mechanical property distributions were determined in these regions. The material within the FSP zone exhibited consistently higher yield strengths, ultimate tensile strengths, and ductilities than the as-cast base metal.

14. SUBJECT TERMS Friction stir processing, Nickel Aluminum Bronze (NAB), raster patterns, transformations, welding, microstructure-mechanical property relationships			**15. NUMBER OF PAGES** 67
			16. PRICE CODE
17. SECURITY CLASSIFICATION OF REPORT Unclassified	**18. SECURITY CLASSIFICATION OF THIS PAGE** Unclassified	**19. SECURITY CLASSIFICATION OF ABSTRACT** Unclassified	**20. LIMITATION OF ABSTRACT** UL

NSN 7540-01-280-5500

Standard Form 298 (Rev. 2-89)
Prescribed by ANSI Std. 239-18

THIS PAGE INTENTIONALLY LEFT BLANK

Approved for public release; distribution is unlimited

FRICTION STIR PROCESSING PARAMETERS AND PROPERTY DISTRIBUTIONS IN CAST NICKEL ALUMINUM BRONZE

Brian P. Rosemark
Lieutenant, United States Navy
B.S., United States Naval Academy, 1997

Submitted in partial fulfillment of the
requirements for the degree of

MASTER OF SCIENCE IN MECHANICAL ENGINEERING

from the

NAVAL POSTGRADUATE SCHOOL
December 2006

Author: Brian P. Rosemark

Approved by: Dr. Terry R. McNelley
Thesis Advisor

Dr. Srinivasan Swaminathan
Co-Advisor

Anthony J. Healey
Chairman, Department of Mechanical and Astronautical Engineering

THIS PAGE INTENTIONALLY LEFT BLANK

ABSTRACT

Cast nickel-aluminum bronze (NAB) alloy is specified for many marine applications, including ship propellers, due to its excellent corrosion-resistance combined with acceptable mechanical properties. Friction stir processing (FSP) can be used to improve the alloy's mechanical properties by localized microstructure modification in the cast material. FSP converts an as-cast microstructure to a wrought condition in the absence of macroscopic shape change, closes porosity, and provides a means to surface harden the castings. The closure of porosity near the surface of the material may shorten the manufacturing and processing time for ship propellers. The surface hardening of cast NAB alloy can be used to increase the wear life of ship propellers. Rockwell Scientific Corporation (now Teledyne Scientific Corporation) supplied three Nickel Aluminum Bronze alloy plates which have been friction stir processed in a raster pattern under a Defense Advanced Research Project Agency (DARPA) project. Each plate had been processed using a different tool RPM and IPM (inches per minute of transverse) combination. Miniature tensile samples were sectioned from the FSP zone and surrounding base metal and mechanical property distributions were determined in these regions. The material within the FSP zone exhibited consistently higher yield strengths, ultimate tensile strengths, and ductilities than the as-cast base metal.

THIS PAGE INTENTIONALLY LEFT BLANK

TABLE OF CONTENTS

THIS PAGE INTENTIONALLY LEFT BLANK

LIST OF FIGURES

THIS PAGE INTENTIONALLY LEFT BLANK

LIST OF TABLES

THIS PAGE INTENTIONALLY LEFT BLANK

ACKNOWLEDGMENTS

I would like to take this opportunity to thank Dr. Alex Zhilyaev and Dr. Chanman Park for their assistance troubleshooting some of the equipment, especially the EDM machine. I appreciate all the help and instruction provided by co-advisor, Dr. Srinivasan Swaminathan, without whom I would not have achieved the precision required with the techniques necessary to successfully complete this thesis. Thank you for being a mentor and a friend. I extend heartfelt thanks to my thesis advisor, Dr. Terry McNelley for his guidance, helpful support and direction. It has been a pleasure working for you. Finally, I would like to thank my wife, Michelle, and son, Jack, for their love, support, and understanding.

THIS PAGE INTENTIONALLY LEFT BLANK

I. INTRODUCTION

A. OVERVIEW

Friction Stir Processing (FSP) is a relatively recent surface engineering technology that can be applied to many metals including Aluminum, Magnesium, Iron, Copper, Titanium, and Nickel-based alloys [1]. When applied to cast metals, FSP can eliminate casting defects such as porosity, and improve the mechanical properties of their surfaces. FSP is an adaptation of Friction Stir Welding (FSW), a solid-state joining process invented by Wayne Thomas at The Welding Institute UK (TWI) in 1991[2]. FSP, as well as FSW, does not melt the metal that is processed, and it is a solid-state process. FSP utilizes a non-consumable cylindrical tool with a concentric pin at one end. The tool is rotated and pressed into a material surface and a combination of frictional and adiabatic heating softens the material, while simultaneously exposing it to a stirring action, resulting in homogenous mixing and refined grain structures [1, 3-5]. The volume of material processed in this manner has improved properties, such as increased strength, ductility, and corrosion resistance [1, 3-5]. FSP is currently being studied for many specific surface engineering applications.

One of the applications that the United States Navy is considering is the application of FSP to cast Nickel-Aluminum Bronze (NAB) propeller surfaces. Due to extremely slow cooling rates, as-cast microstructures are coarse, resulting in reduced mechanical properties. Also, porosity is inherent in the fabrication of cast NAB propeller, and it exists throughout the cast material [6-8]. Currently, fusion weld repair is employed during the propeller fabrication process to fill in the porosity defects. However, after the fusion weld is applied, machining of the propeller surface often uncovers additional porosity. This results in repeated repair cycles that extend the fabrication period up to 18 months, and thereby raising manufacturing costs. Additionally, once a propeller is placed into service, the erosion of the propeller surface can expose porosity which was previously hidden by the surface layer. This results in propeller inefficiency and increased cavitation noise. In extreme cases, it has led to sections of a blade falling off the propeller hub. Current fusion weld repair techniques correct the surface porosity problem, but lengthen the manufacturing process and increases costs. Friction stir

processing the cast propeller has been proposed to eliminate or greatly reduce the fusion weld repair cycle, reducing fabrication time and costs, while enhancing the material properties along the surface.

In a program initially funded by the Defense Advanced Research Projects Agency (DARPA) and currently supported by the Office of Naval Research (ONR), the research being conducted at the Naval Postgraduate School (NPS), in collaboration with other program participants, will provide a correlation between the microstructure and mechanical properties in NAB alloys. The effort will also improve understanding of the microstructure transformations which take place in NAB alloys during FSP, and especially near the interface between the TMAZ (thermo-mechanically affected zone) and the base metal [9-13]. It is anticipated that this program will establish the foundation necessary for the commercialization of FSP, and standardize specific techniques to be utilized in the post processing of U.S. Navy propeller castings. This report adds to the extensive body of work already conducted at the Naval Postgraduate School.

Previous research has identified three combinations of tool RPM (revolutions per minute) and IPM (inches of traverse per minute), which result in a range of heat inputs to the base material. Using those three combinations, Rockwell Scientific Corporation friction stir processed three NAB plates in a rectangular spiral raster pattern, working from the inside out, and keeping the advancing side outward. In a procedure developed at NPS, miniature tensile samples were cut from these three plates by electric discharge machining [9, 10, 12]. The tensile samples were designed to identify the variations in tensile properties and microstructures throughout the stir zone, TMAZ and base metal. Tensile testing was performed and the data was analyzed and compared to previous work. In addition, optical microscopy and secondary imaging in scanning electron microscopy were used to compare microstructures and failure mechanisms.

II. BACKGROUND

A. FRICTION STIR PROCESSING

Friction stir processing provides the ability to thermomechanically process selected locations on a material's surface to enhance specific material properties. FSP is a derivative of friction stir welding, a solid-state process for joining aluminum alloys that are difficult to fusion weld [2]. FSP uses the same techniques as FSW, but FSP is used to modify the local microstructure and not join metals together.

Figure 1 illustrates the FSP process. In step 'a', the non-consumable cylindrical tool is rotated to a predetermined RPM. In step 'b', the tip of the rotating tool is plunged into the workpiece and creates heat. The tool's shape consists of a small diameter pin which is fully inserted into the metal, and a concentric, larger diameter shoulder which is intended to prevent upward displacement of the material at the surface of the workpiece. As the tool penetrates the surface, the rotating pin creates frictional and adiabatic heating. This combination of heating softens the material so that the tool can further penetrate the material. As the tool rotates, it induces a stirring action and material flows around the pin. The depth of penetration is controlled by the tool's shoulder and the length of the pin. Step 'c' in Figure 1 illustrates the shoulder making contact with the material's surface. This expands the hot zone due to heating caused by the rotating tool shoulder. The shoulder constraint on the upward flow of material caused by the stirring action of the pin results in a forging action on the deforming material [1, 5, 14-16]. When the tool is fully inserted into the workpiece, it then traverses across the metal at a specific rate, IPM (inches per minute) as seen in step 'd' of Figure 1.

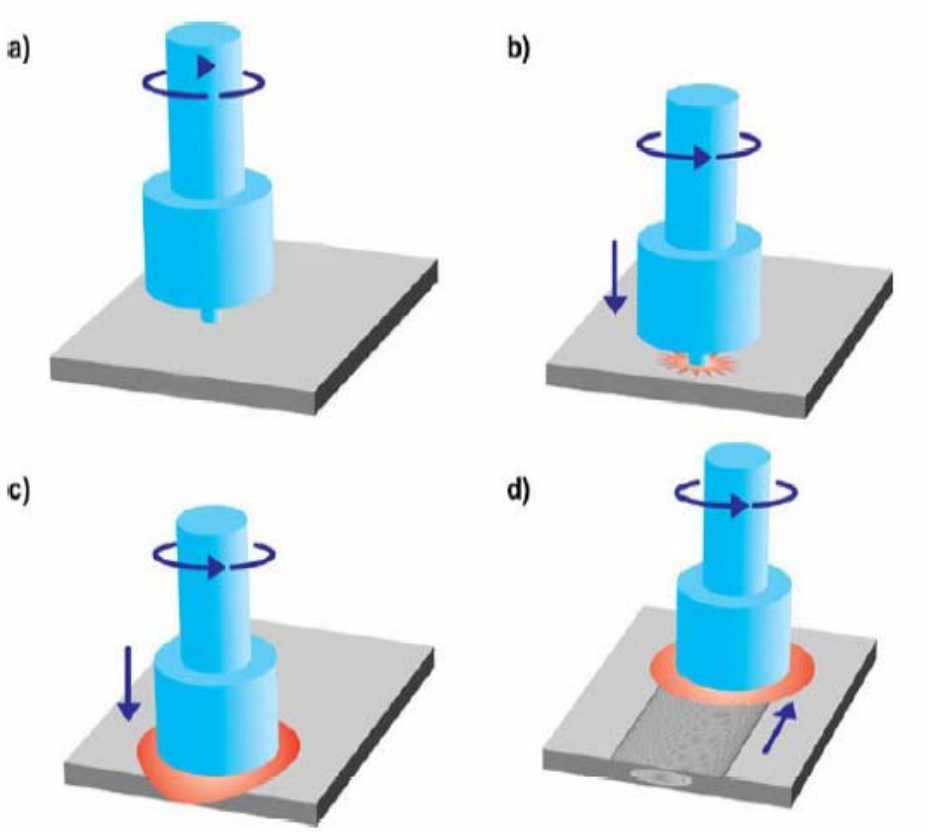

Figure 1. Schematic Illustration of Friction Stir Processing, From [1].

During FSP, the rotating tool provides a continual hot working action, plasticizing the metal within the narrow region surrounding the pin, while transporting the metal from the leading face (advancing side) of the pin to its trailing edge (retreating side). It is important to note that the metal never melts. The peak temperatures achieved in this process are typically 80 to 90 percent of the melting temperature, [3, 4]. After the tool passes by, the processed material cools and exhibits a refined and homogenized microstructure. Essentially, FSP is a thermomechanical metal working process that changes the local properties with minimal influence on the properties in the rest of the material [1].

The hot working process of FSP involves extreme localized strains and strain rates, as well as high temperatures, often around $0.9T_{melt}$. These factors allow FSP to transform the microstructure of cast material to that of a wrought condition. In some alloys, this results in significant increases in material properties such as strength,

ductility, and toughness. Other observed benefits include superplasticity, better weldability, and improved fatigue and corrosion resistance [8]. The area of processed material is often referred to as the "stir zone" or "stir nugget". Below the stir zone is the "thermomechanically affected zone" (TMAZ), where the localized hot working only involved small deformations in the material. Just below the TMAZ is the "heat affected zone" (HAZ) which shares its nomenclature with the same effect found in fusion welds. Similar to fusion welds, the interface between the stir zone/TMAZ/HAZ is a region where ductility loses have been found to exist in NAB. Figure 2 is a montage of optical micrographs which illustrates the stir zone effect for a single pass FSP in NAB alloy.

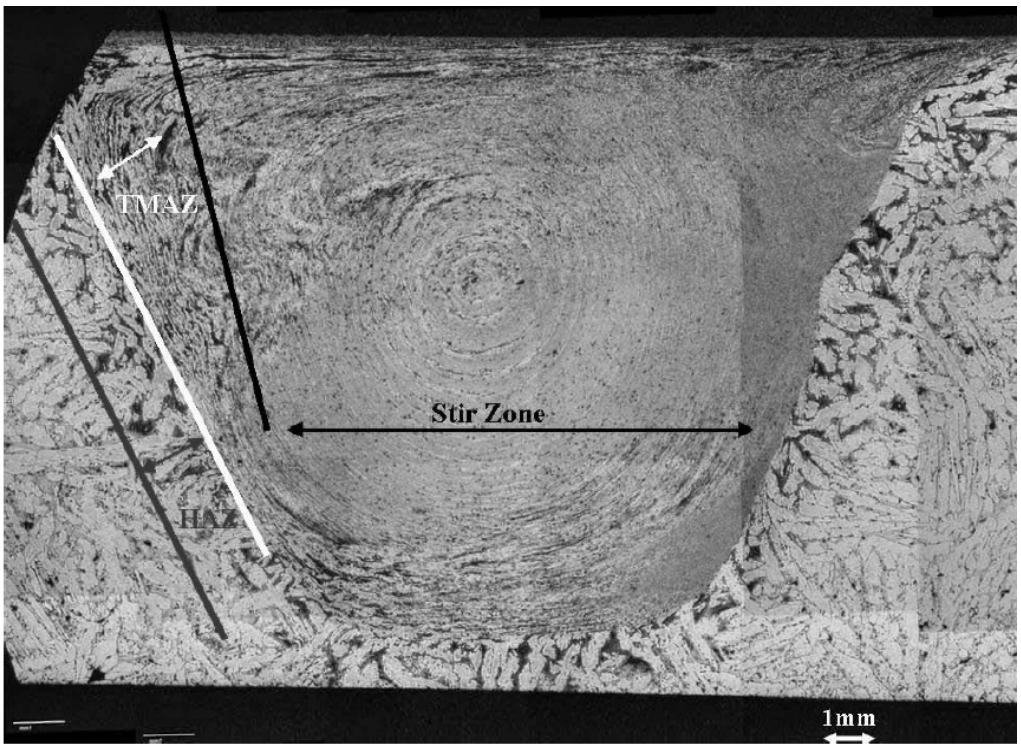

Figure 2. Example of the FSP Zone, From [9].

The tool's geometry is an important parameter in determining the size and shape of the stir zone and its corresponding TMAZ and HAZ regions. The diameter of the tool shoulder can vary from several millimeters to several centimeters, affecting the width of a single pass stir zone. Scroll-shaped grooves on the shoulder surface in contact with the work piece have been used to enhance material flow, increasing homogeneity [1, 16]. Pin

depths for the tools can range up to 100% of their largest diameter, depending on the material, allowing deeper penetration and processing. The pin is always concentric to the shoulder, but includes thread or step-spiral patterns to induce metal flow in the SZ. The speed of rotation, RPM, is an adjustable parameter, but the direction of rotation remains fixed during processing. The direction of travel is defined as the direction the rotational axis of the tool travels, and is not restricted to straight lines. The speed, or traverse rate, of the tool is expressed as inches per minute (IPM). In combination with the tool geometry, the RPM and IPM determine how much heat is generated and introduced into the base metal.

FSP can be used to process large areas by using linear, raster or spiral traversing patterns. An example of raster and spiral patterns is shown in the schematic in Figure 3. These schematics show the tool and the sense of tool rotation [12]. The FSP process is not symmetric about the line of traverse. On the advancing side, the traversing and tangential velocities are added, whereas on the retreating side, the traversing and tangential velocities are subtracted. The advancing side often has steeper gradients in microstructure from very fine and homogenous within the stir zone to relatively undeformed material in the TMAZ. The retreating side usually exhibits more shallow gradients and contain microstructures which are not as refined. Thus, stir zone microstructures are inhomogeneous. Linear raster patterns have advance/advance and retreat/retreat passes, whereas spiral patterns have an overlapping of advancing and retreating sides. The latter tends to increase the likelihood of isotropy of properties in processed regions.

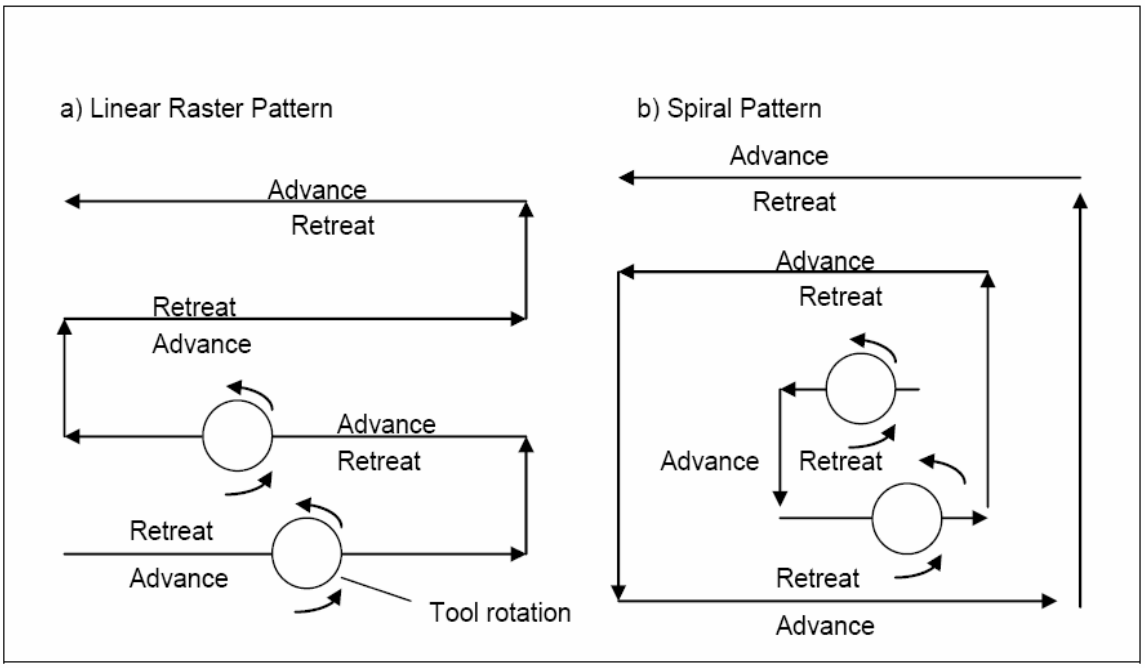

Figure 3. Example of Linear Raster Pattern and Spiral Pattern in FSP, From [12].

B. NICKEL ALUMINUM BRONZE

1. Marine Application

The use of certain compositions of Nickel Aluminum Bronze (NAB) for marine applications have earned it the nickname 'propeller bronze' [17]. It exhibits a unique combination of properties including moderate strength and toughness, and excellent fatigue, corrosion, cavitation, and erosion resistance, which make it an outstanding choice of material for use as naval propellers [8, 17, 18]. These bronzes are Copper based alloys with additions of Aluminum, Nickel, Iron, and Manganese. The specification ASTM B 148-78 designation C95800 prescribes the nominal values for each of the alloy additions [19]. Table 1 lists the nominal weight percentages of the alloying agents within propeller bronze as well as acceptable limits.

Element	Cu	Al	Ni	Fe	Mn	Si	Pb
Min - Max	(min)79.0	8.5 – 9.5	4.0 – 5.0	3.5 – 4.5	0.8 – 1.5	0.10(max)	0.03(max)
Nominal	81	9	5	4	1	-	-

Table 1. Composition Data (wt%) for NAB. From [19].

The problems associated with the use of this material often arise during manufacture. During fabrication, the ship propellers are cast in very large molds. The massively thick sections within the casting can take as long as a week to cool to ambient temperature. This corresponds to a very slow cooling rate on the order of $10^{-3}\,°C/s$ for the thicker sections [20]. This slow cooling rate results in very coarse grains which confer poorer material properties [17, 18]. On the other hand, the thinner sections of the casting experience a faster cooling rate [8]. Due to the wide variation of cooling rates in the various thicknesses, the NAB microstructure sometimes exhibits segregation and gas evolution, resulting in porosity [8, 17]. This porosity creates additional difficulties in the fabrication process requiring fusion welding to fill in the pores, x-ray or ultrasonic inspection, grinding, and possible re-welding. This porosity repair can result in a repetitive cycle of repairs which can create propeller post-cast processing times up to 18 months. FSP is intended to replace the fusion weld repair cycle during the post-cast process. FSP can be used to selectively treat specific regions of the propeller's surface or the entire cast structure. FSP will surface harden the material and close any porosity defects near the surface layer of the propeller. With FSP, the post-cast processing time has been projected to be reduced significantly, saving both time and money. Figure 4 shows a robotic arm performing FSP on a propeller for testing at NSWC Carderock.

Figure 4. FSP Area Processing of a Marine Propeller, From [4].

2. NAB Phases

FSP involves high temperatures, strains and strain rates, as well as a range of cooling rates. These parameters affect the microstructure of NAB and are responsible for its increase in material properties. There are four main phases that can form during the transformation of NAB and these transformation products greatly affect the material properties of the resulting microstructure [3].

a. Beta (β) and Retained-Beta (β') Phases

The β phase is a high temperature solid solution phase of NAB. It is generated during the hot working process in FSP where temperatures exceed $1000\,^{\circ}C$. The β structure is BCC at high temperatures with a lattice parameter of 0.3568 nm [7]. This phase is not stable at ambient temperature; therefore, it must transform into various products as it cools. A variety of transformation products form as a function of cooling rate. Figure 5 outlines the transformations that result during cooling of NAB.

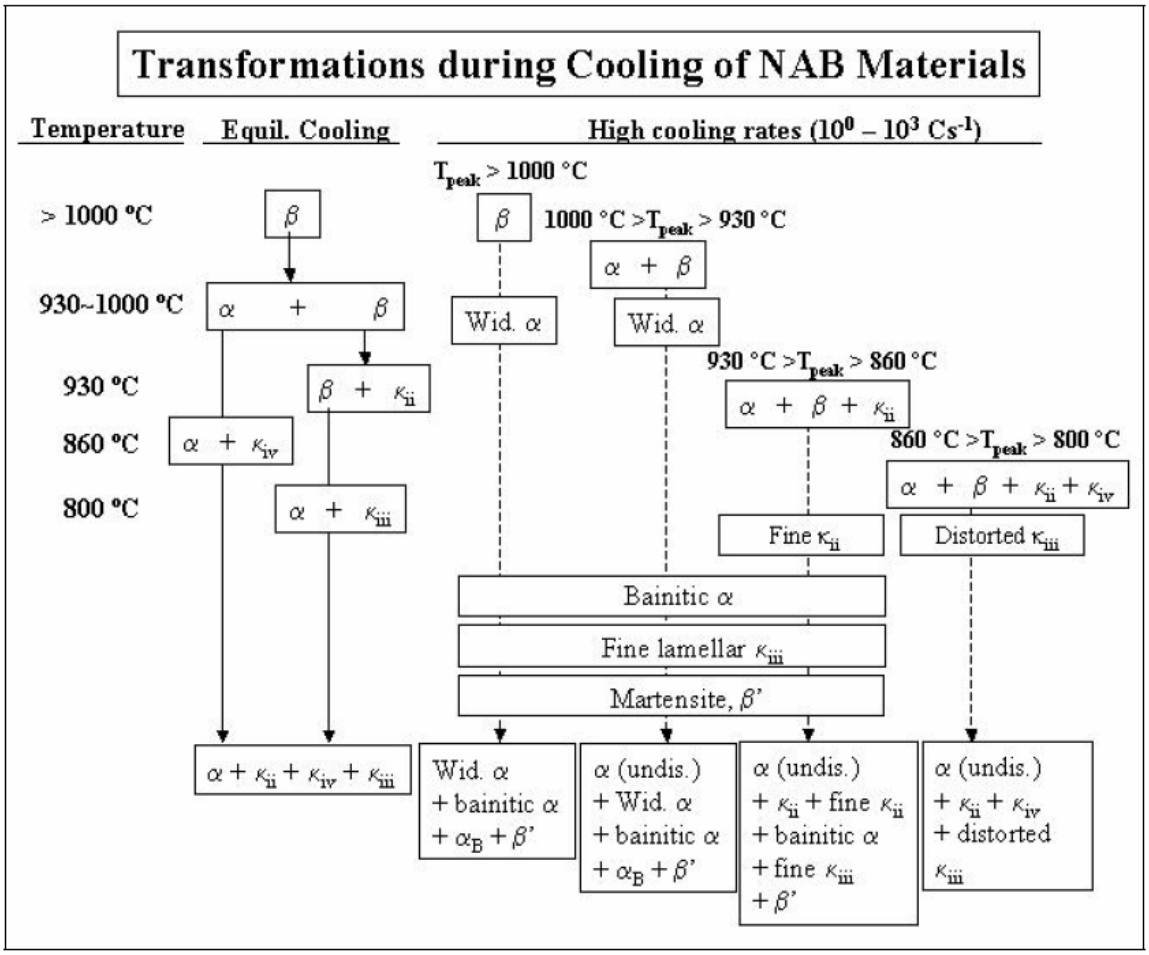

Figure 5. Transformation Products of NAB during Cooling, From[10].

The left side of the figure is for equilibrium cooling, the same cooling which propeller castings are likely to encounter. The very slow cooling rate results in virtually all of the β transforming into alpha (α) and kappa (κ) products [6].

FSP results in considerably faster cooling rates and the material response is outlined in the right hand side of the Figure 5. Depending of the peak temperature attained in the FSP process, the microstructure will resolve into more complex component mixtures that include primary α and β transformation products. The latter structure includes α in a Widmanstatten morphology, β in coarser to finer bainite structures, or martensitic beta (β') [6, 21]. A high density of precipitates form throughout the β on cooling, acting as nucleation sites for the formation of primary α.

The β composition varies throughout the structure depending on the amount of alloying elements that are consumed while forming other phases or particles. In the optical micrographs included in this report, the dark etched constituent represents the various forms of β.

b. Alpha (α) phase

The α phase is the terminal solid solution constituent of NAB. The α structure is FCC at room temperatures with a lattice parameter of 0.364 nm [7]. It is usually the first constituent to form upon cooling of β. The temperature at which α forms is dependant on composition [6]. The composition of the α phase varies during the cooling process as elements are transferred at the α / β interfaces and from within β to form additional phases.

c. Kappa phases (κ)

There are four distinct κ phases which form during the cooling of NAB. They form as a result of the deceasing solubility of iron, aluminum, and nickel during the cooling process [6, 7]. They are all stable at ambient temperatures.

The first kappa phase (κ_i) is usually found in NAB compositions wherein the iron content is greater than 5%, and κ_i may begin forming in the melt [7]. It is generally surrounded by the α phase. The κ_i precipitates are mostly iron rich (FeAl, Fe_3Al) and surround small copper rich particles. Its crystal structure varies between BCC, DO_3, and B2 [7]. When present, κ_i exhibits a large rosette shape, 20-50 microns in diameter, and will etch grey in a micrograph. This phase is not likely to be encountered in the NAB alloy which this report considers.

The κ_{ii} phase is iron rich (Fe_3Al) and has a DO_3 lattice structure [7]. These particles begin to nucleate in the β near α / β interfaces. These particles are usually between 5-10 microns in diameter [7]. These particles tend to form at the same temperature as Widmanstatten α.

The κ_{iii} phase is the only phase that is nickel rich (NiAl). It has a B2 lattice structure [7]. This phase forms upon cooling below $\sqsupset 800\,°C$. The NAB alloys

with the highest nickel concentration tend to form the most κ_{iii}. This phase can take on a globular or lamellar form, but maybe difficult to observe in micrographs since some etching solutions preferentially attack this structure.

The fourth kappa phase (κ_{iv}) has an inter-atom spacing and lattice structure similar to κ_{ii}. These particles are found distributed throughout the α grains, except in a precipitate free zone surrounding primary α grains. The nominal compositions of all the phases found in NAB after equilibrium cooling are listed in Table 2. Figure 6 is a micrograph showing α and κ transformation products of β during equilibrium cooling of cast NAB material.

Phase	Cu	Al	Ni	Fe	Mn
Alpha	85.4	8.3	2.5	2.7	1.4
Beta	85.2	8.7	3.5	1.6	1
Kappa I	8.4	17.5	3	65.6	2.7
Kappa II	9.3	22.2	6.6	53	1.9
Kappa III	12	44.3	31.5	10.2	1.6
Kappa IV	2	18.9	6.1	63.8	2.1

Table 2. Compositions of Phases Present in NAB, In Weight Percent, From [6].

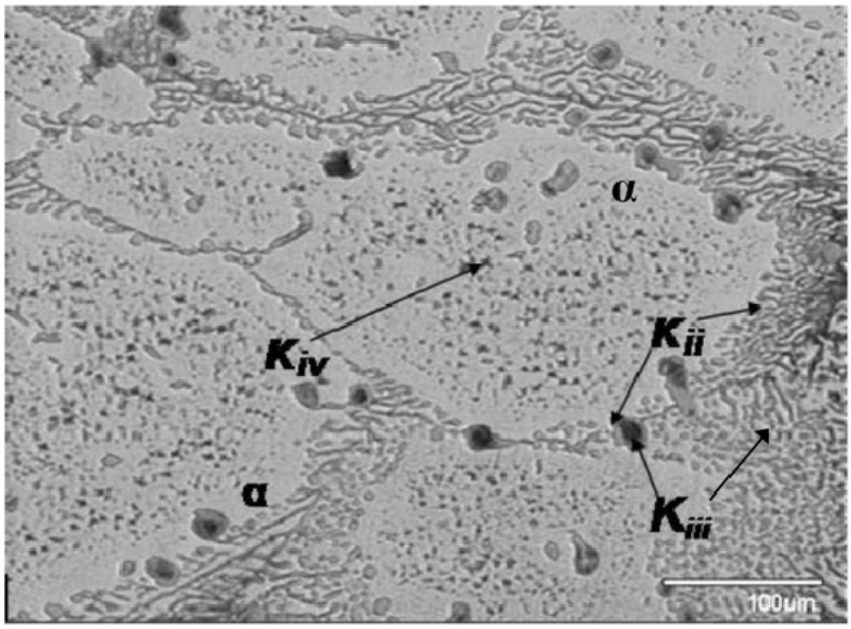

Figure 6. Equilibrium Transformation Products of Cooled Cast NAB, From [10].

3. NAB Microstructure

The above phases contribute to the formation of four primary microstructures associated with FSP of NAB material. The microstructures within and surrounding the stir zone are: a) lamellar, b) fine grain, c) Widmanstatten, and d) as-cast. Figure 7 is a composition of micrographs that show the three unique types of microstructures encountered in FSP (a-c) as well as a comparison (d) microstructure of as-cast NAB material.

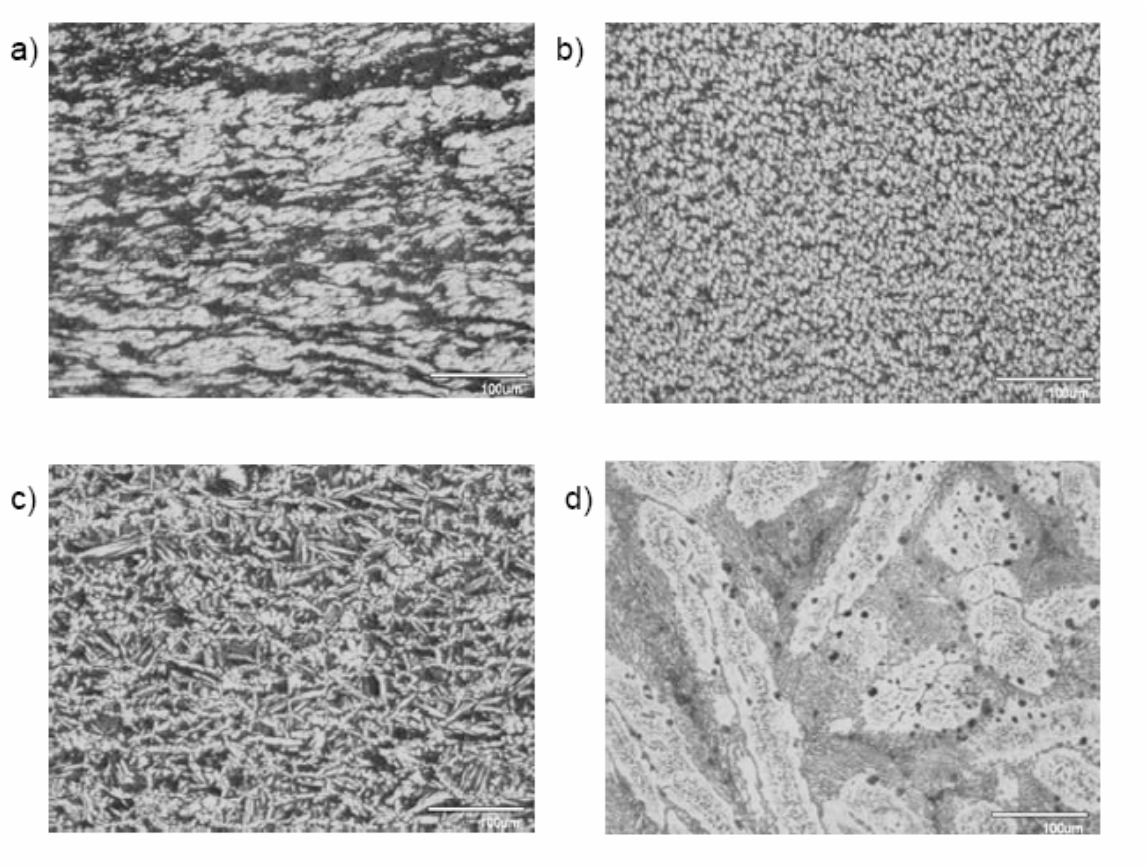

Figure 7. Microstructures created in NAB by FSP, From [10].

III. EXPERIMENTAL PROCEDURES

A. MATERIAL PROCESSING

Three as-cast nickel aluminum bronze plates of similar composition and approximately 32 cm x 14 cm x 3.8 cm in size were subjected to FSP at Rockwell (now Teledyne) Scientific Corporation using a 12.7 mm step-spiral Densimet tool. The plates were processed in a rectangular spiral pattern with the advancing side of the tool kept to the outside of the traverse. The final patterns were 9.8 cm across by 22.5 cm long and successive passes were separated by 4.5 mm. The variable among these three plates is the RPM/IPM combination. Three unique sets of RPM/IPM combinations were used: 1200/2, 1000/3, 800/4, and the plates will be identified here by these designations. These specific combinations corresponded to the transition plan series developed by Mahoney at Rockwell for use in further process development taking place at the Naval Surface Warfare Center Carderock Division, Bethesda, MD [22]. The plates were then provided to the Naval Postgraduate School. Figure 8 shows views of the three plates.

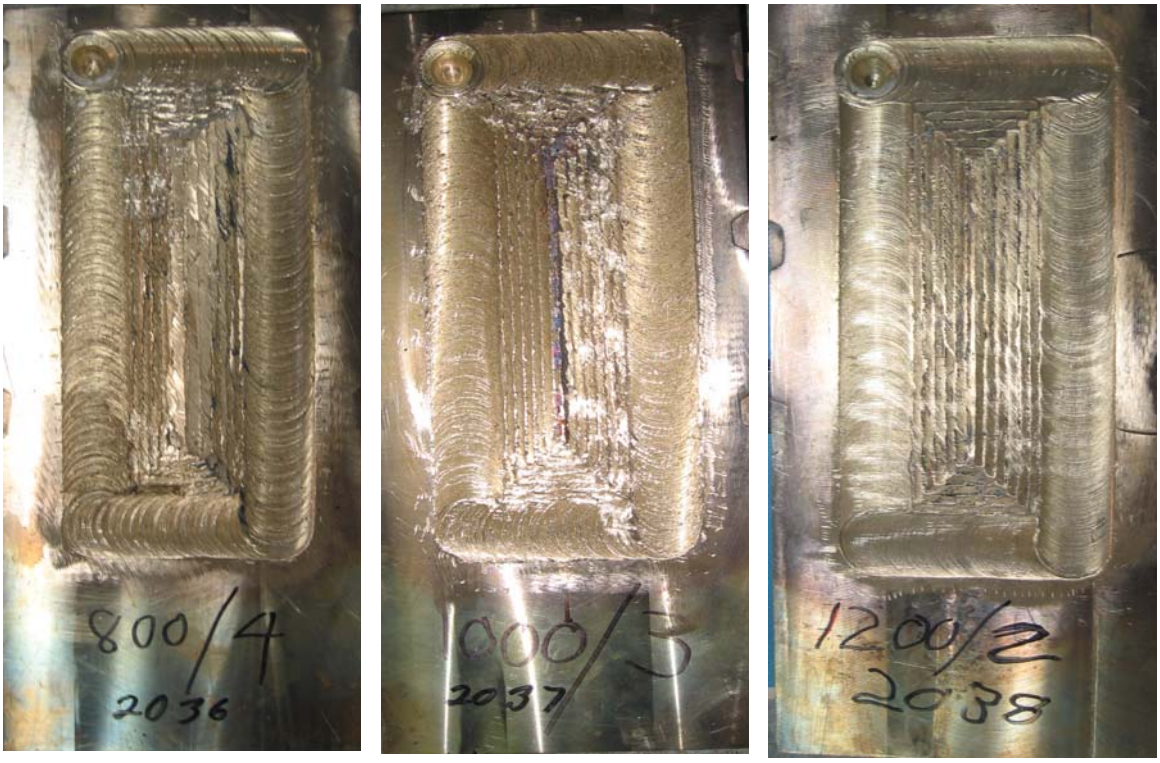

Figure 8. Three FSP NAB Plates before Sectioning.

Three small rectangular pieces of material approximately 0.64 cm x 1.9 cm x 3.8 cm were sectioned from the lower corners of each plate using the Charmilles Andrew EF630 electric discharge machining (EDM) system. These samples were sent to ANAMET Laboratories, Inc. in Hayward, CA for chemical analysis using emission spectroscopy. The composition data is compared to the accepted nominal composition and the ASTM standards in Table 3. The only parameter not within standards is the iron concentration in the 1000/3 plate. It is identified by being underlined in the table.

Element	Cu	Al	Ni	Fe	Mn	Si	Pb
Min-max	(min)79.0	8.5-9.5	4.0-5.0	3.5-4.5	0.8-1.5	0.10(max)	0.03(max)
Nominal	81	9	5	4	1	-	-
800/4	81.0	9.31	4.58	3.51	1.44	0.05	<0.005
1000/3	81.5	9.20	4.44	3.38	1.39	0.05	<0.005
1200/2	81.3	9.17	4.46	3.68	1.24	0.06	<0.005

Table 3. Composition Data (wt%) of NAB Plates Compared to Nominal Values and Standards.

B. TENSILE TESTING

1. Sample Preparation

Miniature tensile samples were cut from the three NAB plates using the computer controlled EDM and consumable brass cutting wire with a nominal diameter of 0.30 mm. The use of the EDM allowed the cutting of the complex tensile specimen geometry without imparting large external forces or excessive heat which may alter a large portion of the material's microstructure. The process of this machining uses intense but localized heat to vaporize a small amount of material and this does create a small, thin heat-affected zone on the outside surface of the cut material. This layer of material is removed by light grinding prior to tensile testing so the effects of EDM are not apparent in the data.

Tensile specimens were obtained from the three NAB plates by, first, using the EDM to cut blocks out of the thick plates in the shape of the tensile specimen. Once all the blocks of one plate had been obtained, the plate was removed from the machine and the tensile blocks were arranged so that they could be individually sliced by the EDM machine to obtain the final tensile specimen with thicknesses of □ 1 mm. Figure 9 gives

the nominal dimensions of the tensile specimens. Figure 10 outlines the steps described above in the EDM machining process of a tensile sample.

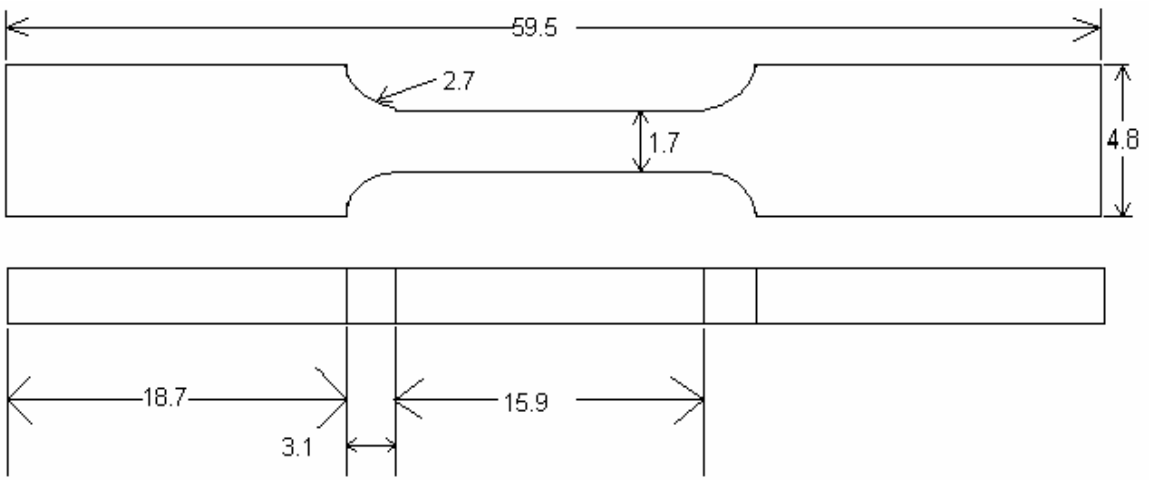

Figure 9. Schematic of Miniature Tensile Specimen. Dimensions in mm, From [10].

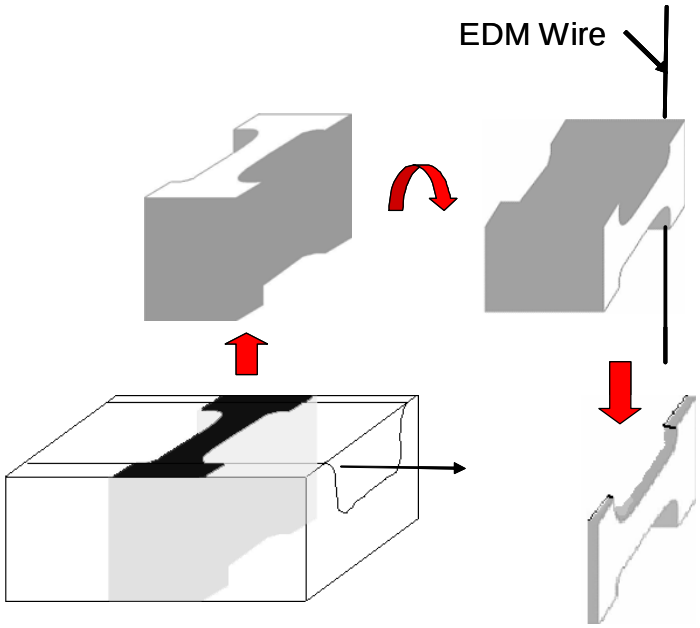

Figure 10. Representation of EDM Machining a Tensile Specimen from FSP Area.

The tensile samples were sectioned to provide specimens that would permit the identification of the distribution of the mechanical properties and microstructures that fall within the stir zone and TMAZ interface. Each tensile block was sliced so that the material properties of yield strength (σ_y), ultimate tensile strength (σ_{UTS}), and ductility

can be identified as a position of depth within the volume of processed material and base-metal. Four tensile blocks were sectioned from both the 800/4 and the 1000/3 plates. Six tensile blocks were sectioned from the 1200/2 plate. The blocks are labeled to reflect their orientation with respect to the FSP tool's local direction of travel. Figure 11 shows pictures of the three plates after the tensile blocks have been cut, L for longitudinal or T for transverse. Thus, L denotes a block cut such that sample tensile axes will be parallel to the local travel direction and T refers to sample tensile axes transverse to the local travel direction. Each block is also labeled with a number: 1, 2, or 3, which indicates its position from the outside edge. The blocks labeled 1 are along the outside of the processed zone, and represent the last pass which was performed. The blocks labeled 2 represent an area in the middle of the process zone which has been processed multiple times. The blocks labeled 3 represent the geometric center of the pattern; these are at the location of the first pass which was performed on the material. Each tensile sample is labeled with the plate and block from which it had been cut, as well as a letter indicating its depth within the stir zone. The surface specimen was labeled 'a', and the resulting specimens are labeled with a letter corresponding with its distance from the surface. Of note, the specimens on the surface, 'a', were not used for tensile testing. These represent a volume of material which would be removed during the polishing/grinding process of any material which requires a smooth finish. Over 200 tensile samples were prepared for this research.

The cutting wire of the EDM is 0.30 mm in diameter. As the wire cuts through the material, it erodes a kerf slightly more than the 0.30 mm of its diameter. As a consequence, the physical dimensions of the tensile specimens have some variation. The program controlling the EDM cutting slices the specimen blank every 1.4 mm. This results in a tensile specimen which has had material eroded away from both surfaces. The end result is a specimen about 1 mm in thickness, with the centers of successive specimens always separated by 1.4 mm. In expressing distances from the surface of the plate, the 1.4 mm spacing between the tensile specimen's centers was used in the following results.

To remove the outer layer of material which had experienced intense heating and perhaps phase transformation, each face of the tensile samples was ground with 400 grit

SiC paper on the ECOMET 4 grinding/polishing until the gauge length was smooth. Then, the gauge thicknesses were ground by hand with the same paper. Copious amount of water was used on the wheel to prevent heat build up within the material.

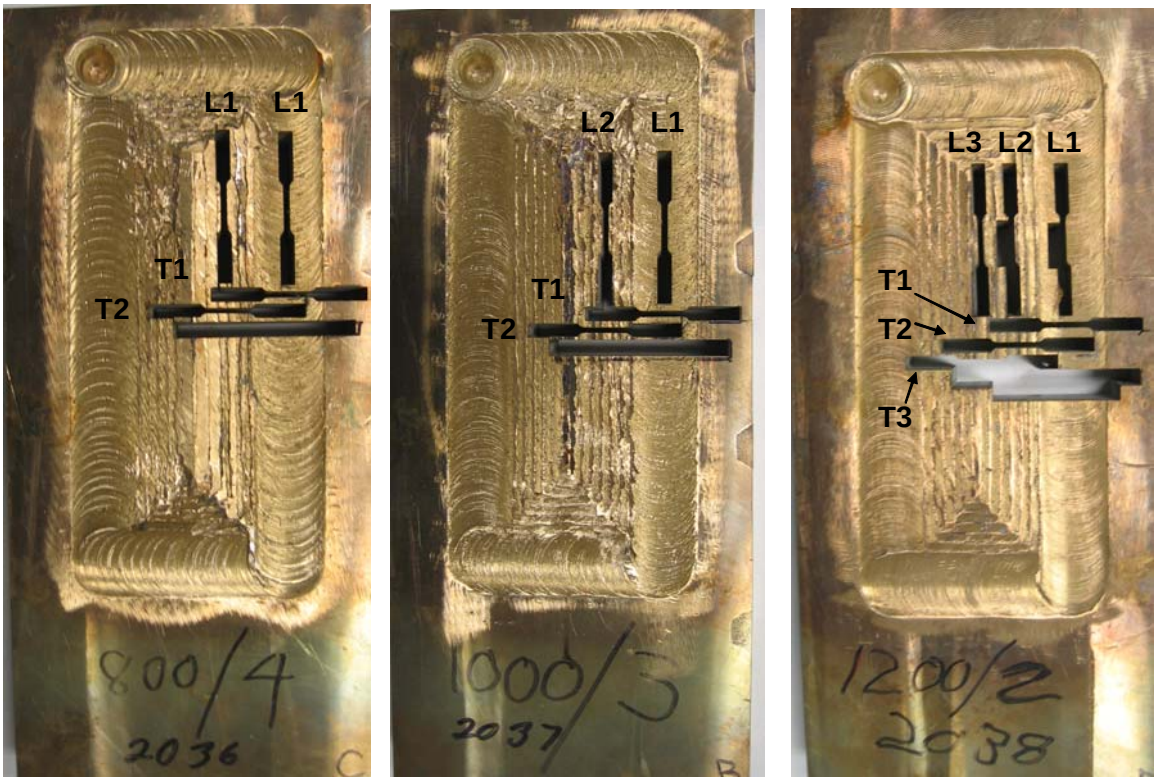

Figure 11. Plates After Cutting Tensile Blocks.

2. Mechanical Testing

Tensile testing was performed on 198 samples using a computer controlled INSTRON Model 4507 tensile machine with GPIB interface control and Series IX data collection software. A constant cross head displacement rate of 0.954 mm/min was used for all tensile tests. The tensile samples were mounted into screw platen grips with great care to ensure consistent sample alignment for axial loading. Misalignment off the primary axis would induce a torque and create a tearing effect in the gauge length. A universal joint was used between the load cell and the upper grip to aid in tensile sample positioning. Before each test, the load cell and extension length were reset and balanced. Each tensile sample's gauge length, thickness and width were measured prior to testing due to variances between each sample which result after grinding and this data was fed into the computer software. Each sample was tested to failure by constant displacement

of the lower fixed grip in the downward direction. For each run, engineering stress, engineering strain, load cell, and crosshead displacement data were gathered at 5 Hz and recorded in an ASCII 2 format file. The files were then imported into a MATLAB m-file using MATLAB Version 7.1 for analysis. This analysis compensated for the elastic response of the machine frame, its grip, the load cells, and the universal joint. This step was required because the miniature tensile samples were too small to fit with available extensometers. Figure 12 shows a representative stress versus strain graph obtained by these procedures.

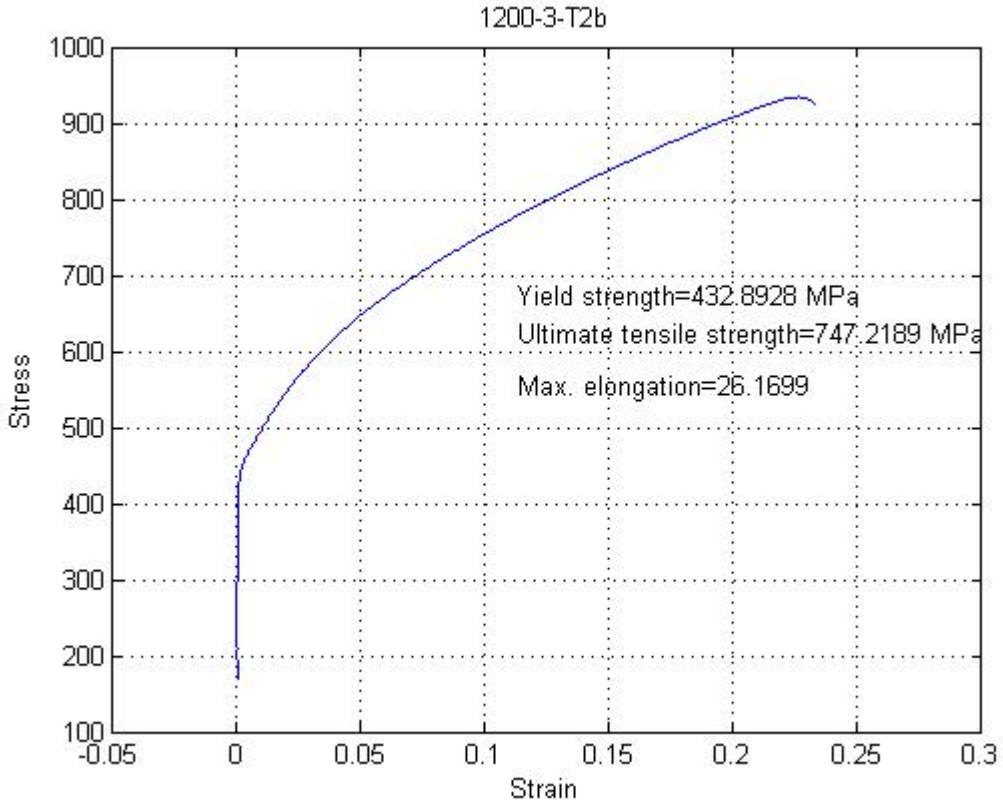

Figure 12. Representative Stress versus Strain Graph. This is for sample 1200-3-T2b.

C. OPTICAL MICROSCOPY

Samples selected for optical microscopy were sectioned from the three different plates using the EDM machine. The samples were polished in several steps using Buehler ECOMET 4 and 3 grinding/polishing wheels. Grinding began on the ECOMET 4 wheel using 800 grit SiC paper for 60 seconds at 80 RPM, adding a copious amount of water to prevent frictional heating of the material. The process continued on the

ECOMET 4 wheel using progressively finer grit SiC paper. The SiC papers used were 800, 1000, 2400, and 4000 grit. After these first four stages of grinding, the samples were rinsed with water and then polished on the ECOMET 3 polishing wheel. Three stages of polishing were used on this wheel. The first stage used Buehler's 3 micron metadi diamond oil-based suspension. The samples were polished with this suspension for 15 minutes at 120 RPM and then ultrasonically cleaned in methanol for 10 minutes. They were then dried with a hot air gun (hair dryer). Stage 2 polishing used Buehler's 1 micron metadi diamond oil-based suspension. Again, samples were polished for 15 minutes, but at 140 RPM, and then ultrasonically cleaned in methanol for 10 minutes. After drying they were polished with Buehler's 0.05 micron water-based colloidal silica suspension. Polishing during this last stage was continued until there was a scratch-free, mirror surface, typically requiring 15 minutes at 100 RPM. After this last stage of polishing, the samples were rinsed in water and then ultrasonically cleaned in acetone for 10 minutes. They were dried and then immediately etched.

Two etching solutions were used. The first solution consisted of 40 ml water, 40 ml ammonium hydroxide, and 2 ml hydrogen peroxide. The second solution was a mixture of 60 ml water, 30 ml phosphoric acid, and 10 ml hydrogen peroxide. The samples were etched by immersing them in the first solution for 1-2 seconds, followed immediately by removal and rinsing with copious amount of water. They were then immersed in the second solution for 1-2 seconds, removed and again rinsed with water. The samples were then dried and viewed under an optical microscope.

Optical Microscopy (OM) was used to evaluate the grain structure and morphologies of prepared cross sections containing FSP material. Optical microscopy was conducted using a Carl Zeiss JENAPHOT 2000 Inverted Reflected Light photomicroscope. The microscope provided visual output via a PULNIX TMC-74-CCD camera. The digital output was saved with SEMICAPS photo capturing and measurement software. Montages of cross sections were prepared at 48x magnification. In addition, selective montages were created at 290x magnification. Finally, several micrographs were taken at 370x magnification for a closer examination of microstructure.

D. SCANNING ELECTRON MICROSCOPY

Scanning Electron Microscopy (SEM) in the secondary imaging mode was conducted on fractured tensile specimens to identify the predominant fracture mode of the failed tensile samples. The SEM was the Topcon Model SM-500/510 SEM. Thirty-two tensile samples were observed. These included high strength/high ductility samples, base plate samples, samples within the TMAZ, and those samples that displayed low ductility in regions where high ductility was anticipated.

IV. RESULTS AND DISCUSSION

Results of optical microscopy, tensile testing, and SEM fractography of NAB material processed by FSP is presented in this chapter. The FSP involved the three RPM/IPM combinations that were identified as part of the transition plan [22]. The main focus here is a comparative analysis of those three RPM/IPM combinations.

A. MICROSTRUCTURES

A specimen was sectioned from each of the three plates to reveal a plane normal to the direction of tool travel and this specimen was prepared for optical microscopy. Below are three montages of optical micrographs produced at 48x magnification for comparison among these material and processing conditions. In each figure, the right side represents the advancing side of the tool. Figure 13 is a montage of the plate processed with the 800/4, RPM/IPM combination. Figure 14 is a similar montage of the 1000/3 plate and Figure 15 of the 1200/2 plate.

Figure 13. Montage of Optical Micrographs for the 800/4 Processed Conditions.

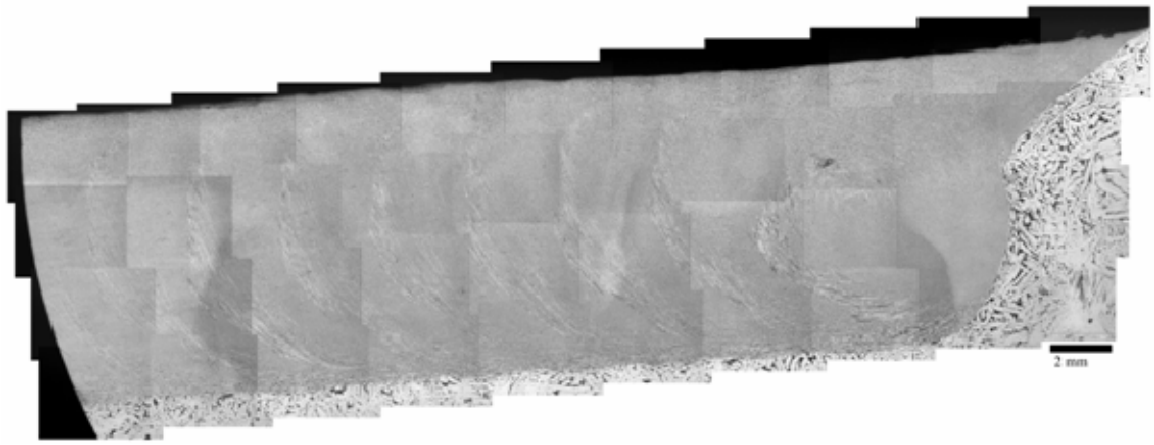

Figure 14. Montage of Optical Micrographs for the 1000/3 Processed Conditions.

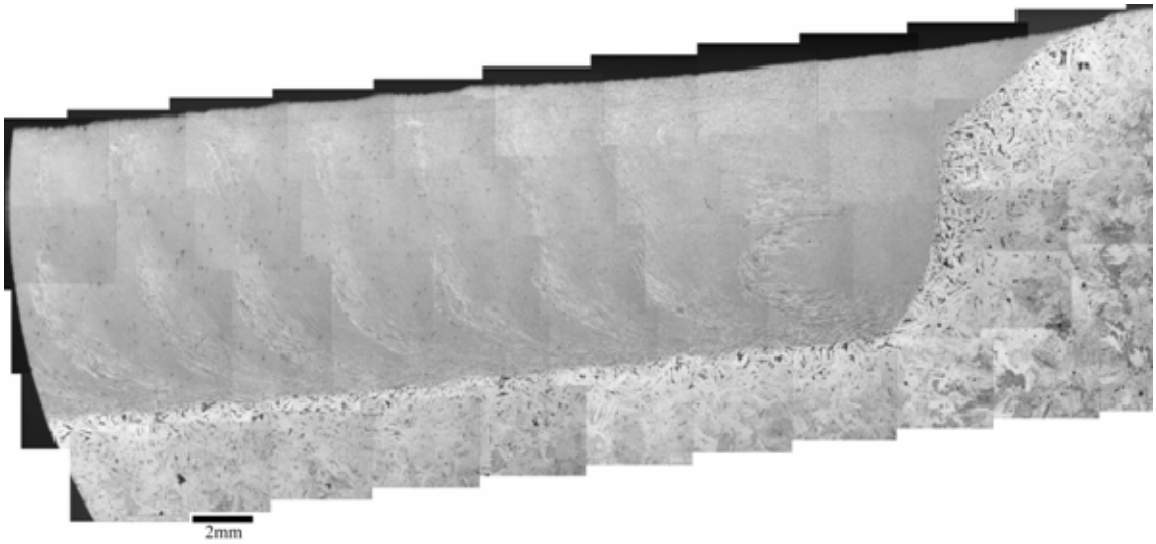

Figure 15. Montage of Optical Micrographs for the 1200/2 Processed Conditions.

There are no significant differences among these three montages despite the range of processing conditions. The 1200/2 material should have experienced a higher heat input than the 1000/3 condition, which in turn, should have had a higher heat input than the 800/4 condition. Nevertheless, all three conditions appear to have similar TMAZ and HAZ regions. All three appear to be much finer than the as-cast material and to exhibit microstructure variation consistent with an offset of 4.5 mm.

The similarities among these data need further discussion. First, the depth of the stir zone, 12 mm, is equal in all the figures. This reflects that the same tool was used during processing under displacement control. Second, within the stir zone, there are

several ‘bands’ of fine grained microstructure apparent. These bands correspond to the multiple passes which the FSP tool made to produce the rectangular spiral pattern. The overall microstructure is remarkably homogenous and the bands are evident only on the lower scales of magnification. Next, corresponding to the last pass, there are swirl patterns within the stir zone. These have also been called ‘onion ring’ patterns. These swirl zones are about 6 mm in diameter, and are the least homogenous feature within the stir zone. Multiple pass processing appears to break up and disperse these features.

The TMAZ is of similar dimension in all the montages and occurs at a depth of 12 mm $\pm$ 0.5 mm. Likewise, the thickness of the HAZ is only about 1 mm at the bottom of the stir zone. This is not true for the size of the HAZ on the sides of the material. Due to the NAB material’s higher thermal conductivity, a large portion of heat was conducted on sides of the material, creating a larger HAZ. The length of the HAZ is as much as 3 mm on the outward edges of the processed zone. Again, the HAZ is of similar dimensions in all three process conditions.

B. TENSILE TESTING RESULTS

Previous studies have shown that a region of low ductility exists near the stir zone/TMAZ/HAZ interface in NAB materials. It was suggested that this is caused by the formation of low ductility martensitic transformation products of β produced by the heating and subsequent cooling rates. Additional studies have discovered that the same region of low ductility exists in fusion welds of NAB materials [10]. In addition, studies involving FSP in single pass and linear raster pattern processing have found low ductility in the transverse direction. Figures 16-19 are plots of σ_y, σ_{UTS}, and ductility from 198 tensile tests conducted on these three plates. These plots were created by compiling the material property data from the 198 stress versus strain curves calculated from each tensile test. Figures 16-19 illustrate the variation in material properties with depth in the stir zone. Each figure represents the complete set of data for one tensile block, i.e. L1, L2, T1, or T2. These graphs represent the bulk of this program of investigation in terms of the time required to produce them. The data points show how the material properties change as the depth increases through the stir zone, transitions the TMAZ, transitions

through the HAZ, and progression into the base metal. The values on the far right of the curves, representing depths 16 mm and beyond, are consistent with values obtained for the base metal.

The values of σ_y □ 225 MPa (33Ksi), σ_{UTS} □ 450 MPa and % elongation □ 10-12% are consistent with data in the literature for as-cast and slowly cooled NAB [8, 17]. The L1, L2 and T2 data illustrate clearly the effect of FSP on stir zone properties. Thus, the σ_y in all three cases is approximately doubled, increasing from around 225 MPa to values from 400-500 MPa (58-72 Ksi) within the stir zone.

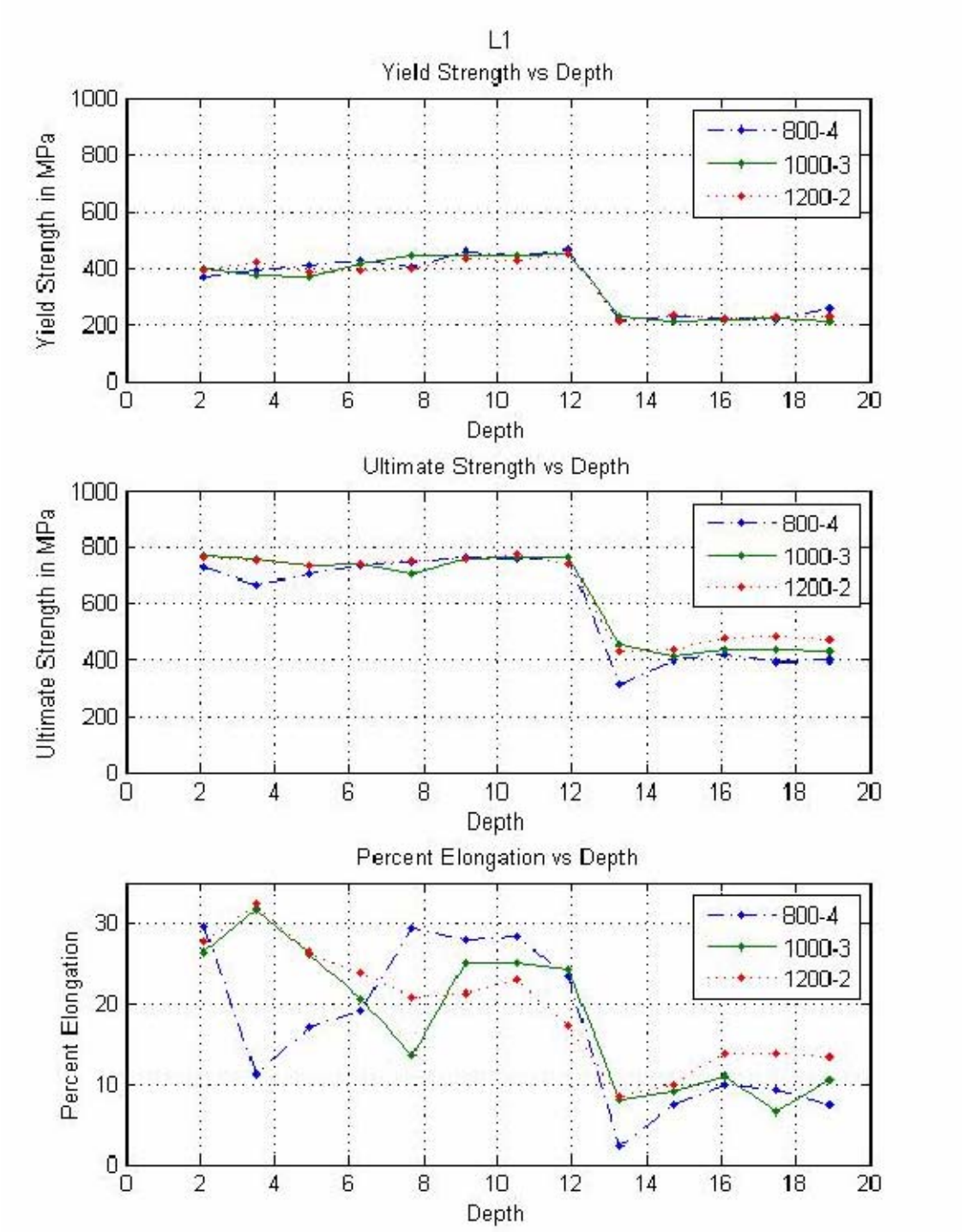

Figure 16. Comparing Material Properties vs. Depth in Tensile Blocks L1; for NAB material FSP with three different RPM/IPM Combinations.

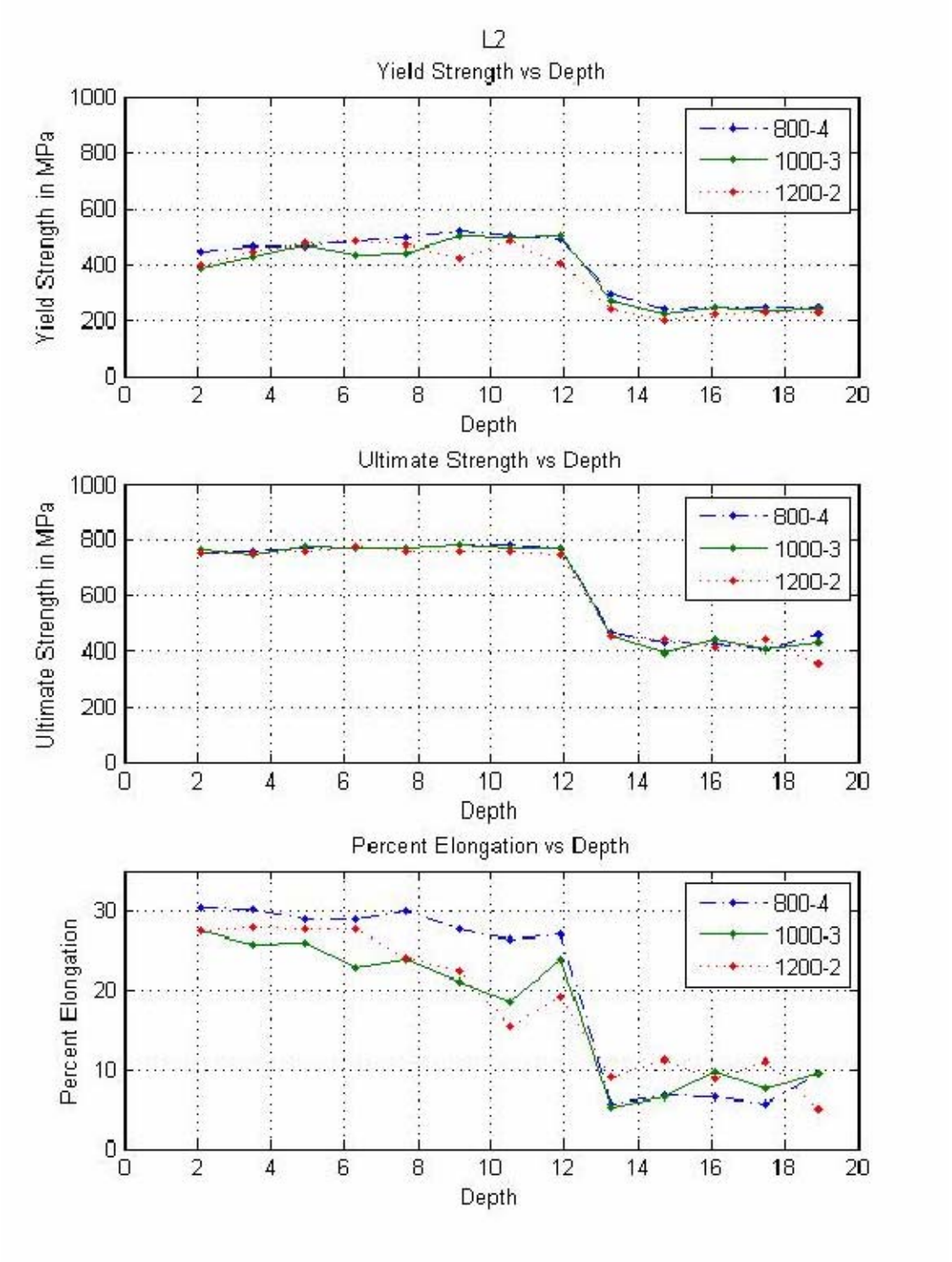

Figure 17. Comparing Material Properties vs. Depth in Tensile Blocks L2; for NAB material FSP with three different RPM/IPM Combinations.

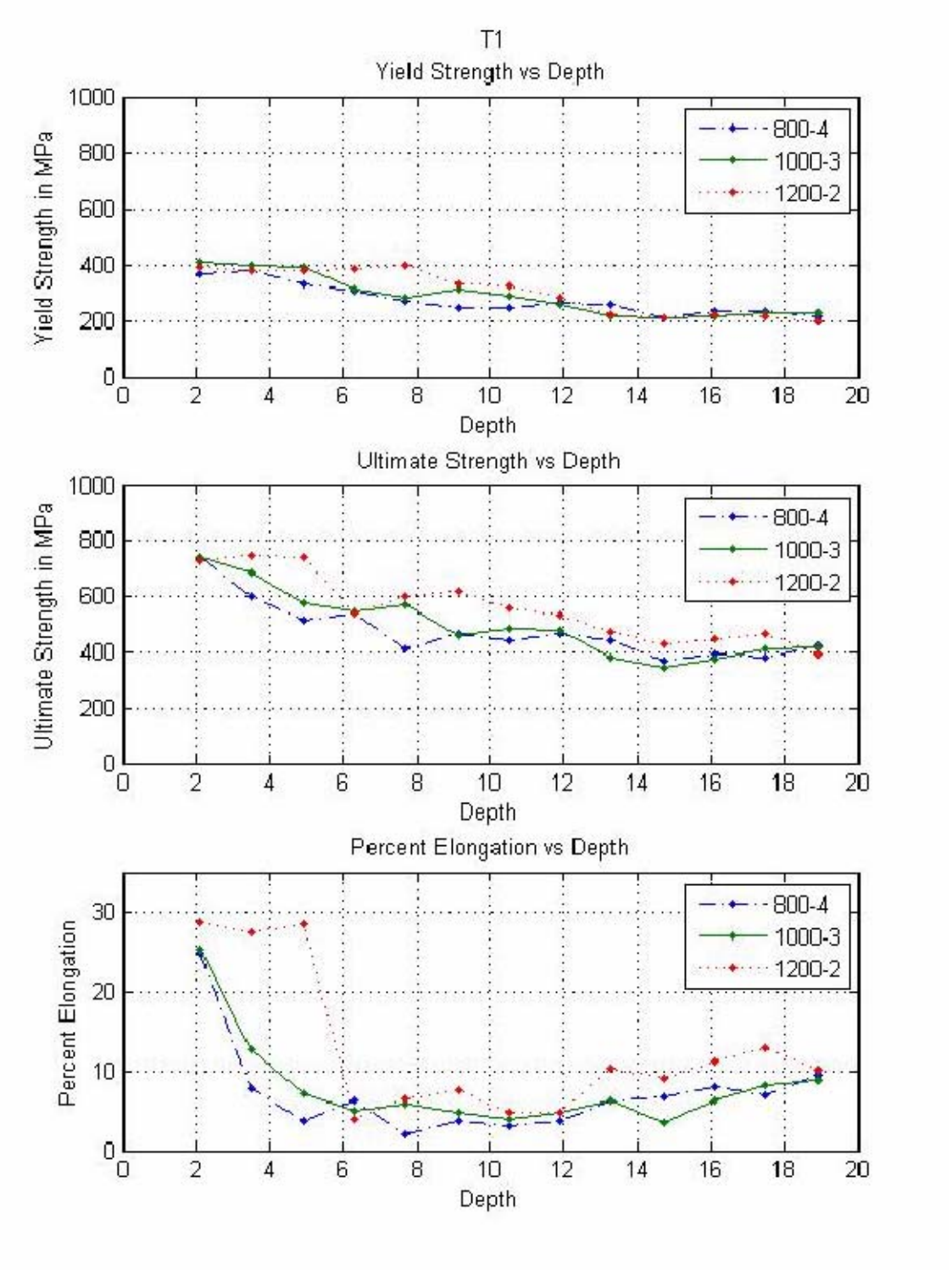

Figure 18. Comparing Material Properties vs. Depth in Tensile Blocks T1; for NAB material FSP with three different RPM/IPM Combinations. See report for discussion on these unique results.

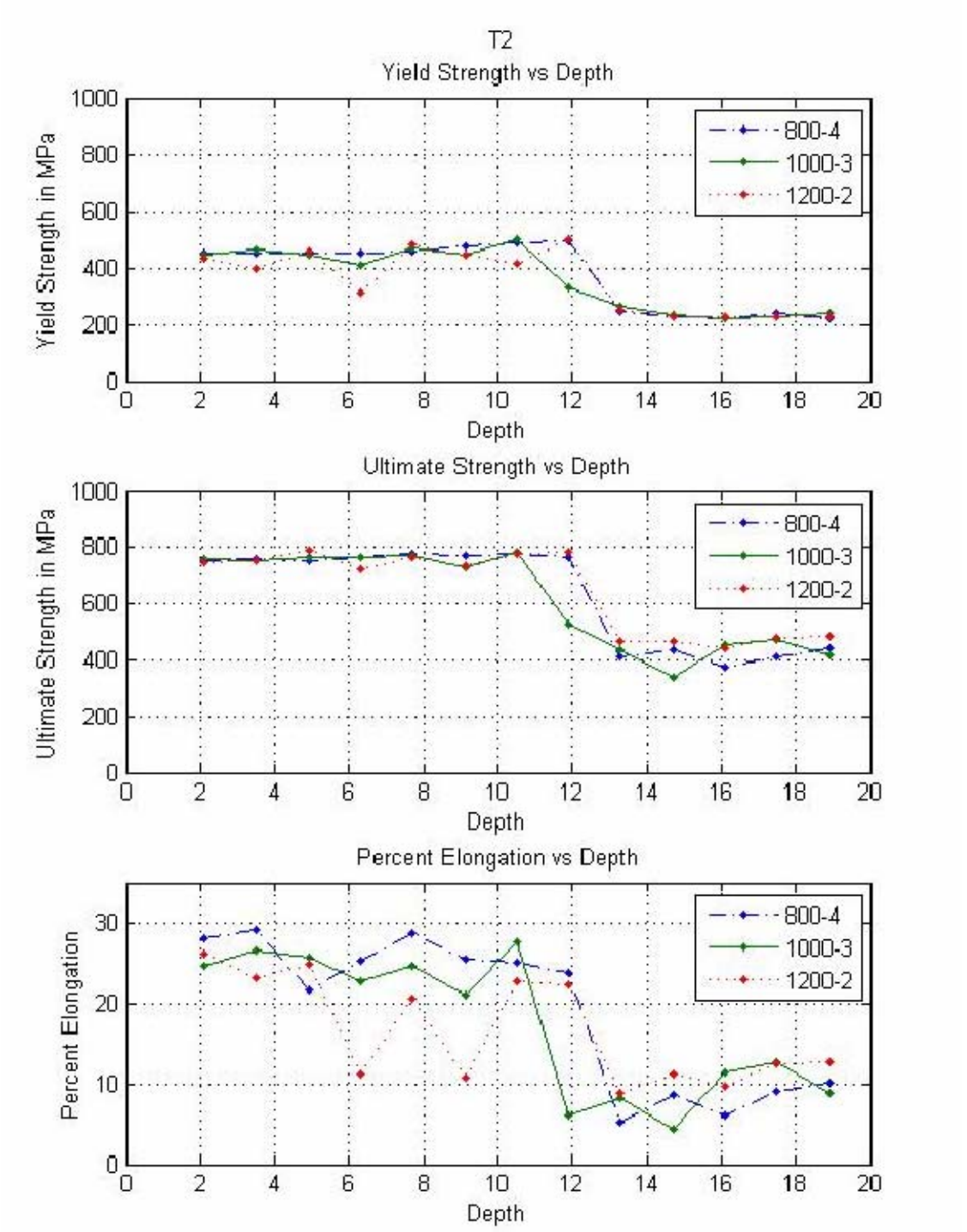

Figure 19. Comparing Material Properties vs. Depth in Tensile Blocks T2; for NAB material FSP with three different RPM/IPM Combinations.

The microstructure in this region consists mainly of fine, equiaxed, α phase grains and the dark-etching transformation products of β phase that, together, provide strengthening. Of note is the uniformity of σ_y obtained from the miniature tensile samples in the L1, L2 and T2 tensile samples.

Likewise, σ_{UTS} is uniform and almost doubled as a result of FSP. All conditions exhibit $\sigma_{UTS} \approx 750-790$ MPa (109-115 Ksi) in the stir zone, with little variation until reaching the bottom of this region. The data from figures 16, 17 and 19 suggest that FSP enhances strength with little dependence of properties with FSP parameters, suggesting a wide window of processing parameters may be employed.

Ductility (measured as percent elongation) is of particular concern in NAB. In prior research, ductility has increased in some areas within the stir zone only to fall dramatically in other sections. The goal in this research is to evaluate the rectangular spiral pattern employed to process these three plates in anticipation that this will alleviate some of the ductility problems identified in certain areas of single-pass FSP material. Figures 16, 17, and 19 show dramatic results: ductility, on average, increased from 10-12% to 25-30%. Although the percent elongation is not uniform, only 8 data points out of 71 samples fall below 20% ductility, resulting in only 11.3% of the samples not achieving 20% or more in ductility. Even then, none of the samples were below 10% ductility within the stir zone. In the above statistics, the samples from blocks T1 were not considered for reasons to be discussed later. Surprisingly, ductility values were consistently high in the transverse direction, i.e. for the T2 tensile block.

Figure 18, pertaining to the tensile samples from the T1 blocks, needs further explanation. The tensile samples of T1 were cut so that material properties could be determined within the last pass which the FSP tool made during processing. Figure 11 indicated the gauge length of the tensile samples was intended to lie within the processed zone on the surface of the plate. Here it is important to recall that the processing on the plate's surface is caused by the tool's shoulder, not by the pin. As can be seen in the montages of optical micrographs in Figures 13-15, there exists a lip or ridge of material and a steep gradient with depth. This lip only goes down 4 mm. The gauge length of the

T1 tensile samples starts above this gradient, and this accounts for the initial high values of material properties, but as the depth of the tensile sample increases, the gauge length now contains both stir zone material and base material that has experienced TMAZ/HAZ effects. As a result, the ductility quickly drops to values similar to those found in other blocks near the 13.3 mm data point. The σ_y and σ_{UTS} values slowly drop to the base metal condition instead of exhibiting the distinct drop that ductility experiences. Altogether, the T1 results suggest that the low ductility in these samples is the result of strain localization due to the 'composite' nature of these samples. The gauge length comprises both stronger stir zone material and weaker TMAZ/HAZ or base metal. These later features yield and deform to failure before yielding of the stir zone, and result in localization of strain during deformation.

Figure 20 is a macro photo to help visualize such effects in tensile sampling as well as to help understand the percent elongation found in several samples. The top tensile sample shows the gauge length prior to testing, as well as the rough surface created during EDM machining. The sample second from the top again shows the original gauge length but this sample has been polished to remove the surface roughness which could act as a stress concentrator and thus invalidate the data. The middle tensile sample is taken from a region in a NAB plate which consists entirely of base metal. It experienced a percent elongation of 10%. Note the 'orange peel' effect across the entire gauge length. This feature will help distinguish base metal from the processed metal. The indentations at the ends of the tested samples are from tightening the samples in the load grips. The two lower tensile samples are from the stir zone, one from a blank in the longitudinal orientation, the other in the transverse orientation. They exhibited ductilities of 28% and 25% respectively. The deformed gauge sections appear smooth and are free of the 'orange peel' effect, reflecting the finer stir zone microstructure.

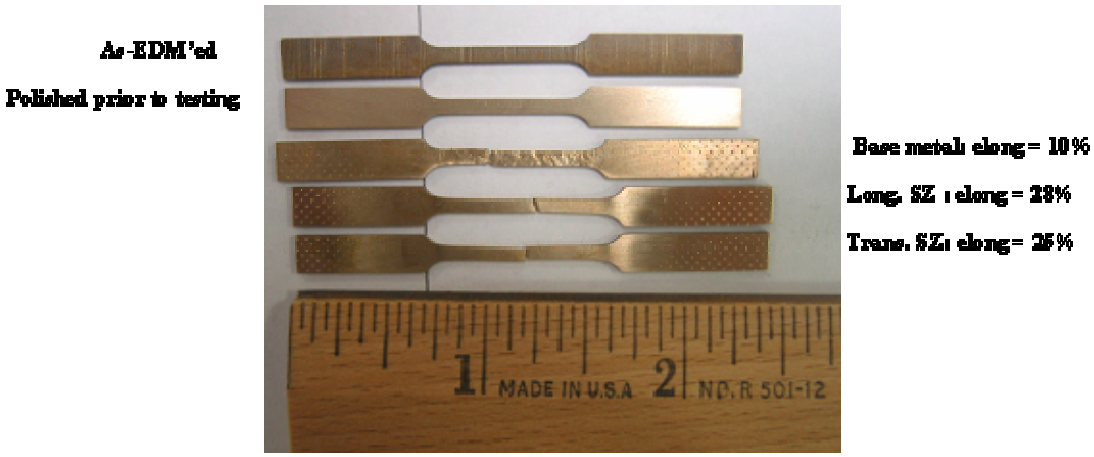

Figure 20. Photo of Tensile Samples.

Figure 21 shows the tensile specimens for 1000/3 T1 block. These data show how the tensile specimens after 'b' failed at similar locations (c-i). The location of failure in 'c-i' includes the 'orange peel' effect on both sides of the failure. This indicates that the specimen failed in the HAZ or base metal region and not in the stir zone or at the advancing side interface. The presence of the high-strength, stir-zone material in the gauge length effectively shortened the gauge length's distance, and largely explains the low ductility. Note that once the stir zone material is replaced in the gauge length, the tensile sample fails in other locations.

It is important to reiterate that no significant differences in material property data result due to the unique RPM/IPM combinations used to process this NAB material.

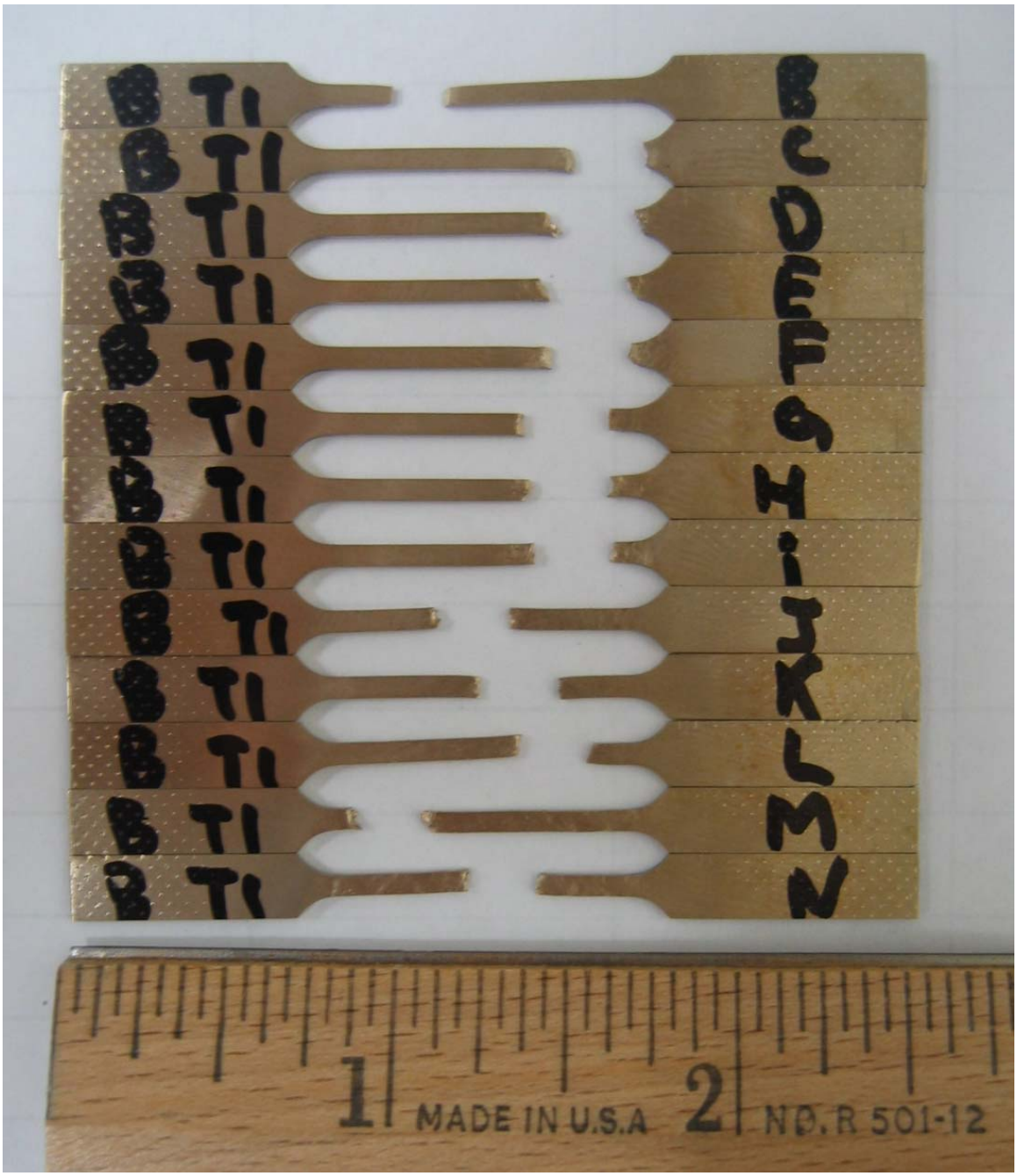

Figure 21. Tensile Specimens for 1000/3 T1.

Figure 22 presents the data obtained from the L3 and T3 tensile blocks sectioned from the 1200/2 processed plate. Only the 1200/2 was sectioned in this location. In the L3 data, the material properties are similar to those as experienced in the other tensile blocks and plates. However, in the T3 data the material properties are variable with

depth in the stir zone and indicate low ductility values for stir zone samples T3-b thru T3-h. Visual examination of the plates in the location of the T3 samples suggest that there may be an advancing side interface at the location of the first pass, and that this interface is not removed by the subsequent passes. Also, this region will experience higher cooling rates than later portions of the spiral raster. A more complete analysis of this region is required.

Finally, low ductility was noted in all sample series at locations just below the stir zone. Similar low ductility values were obtained beneath weld metal in the HAZ of a fusion weld overlay. This will be examined in more detail in a later section.

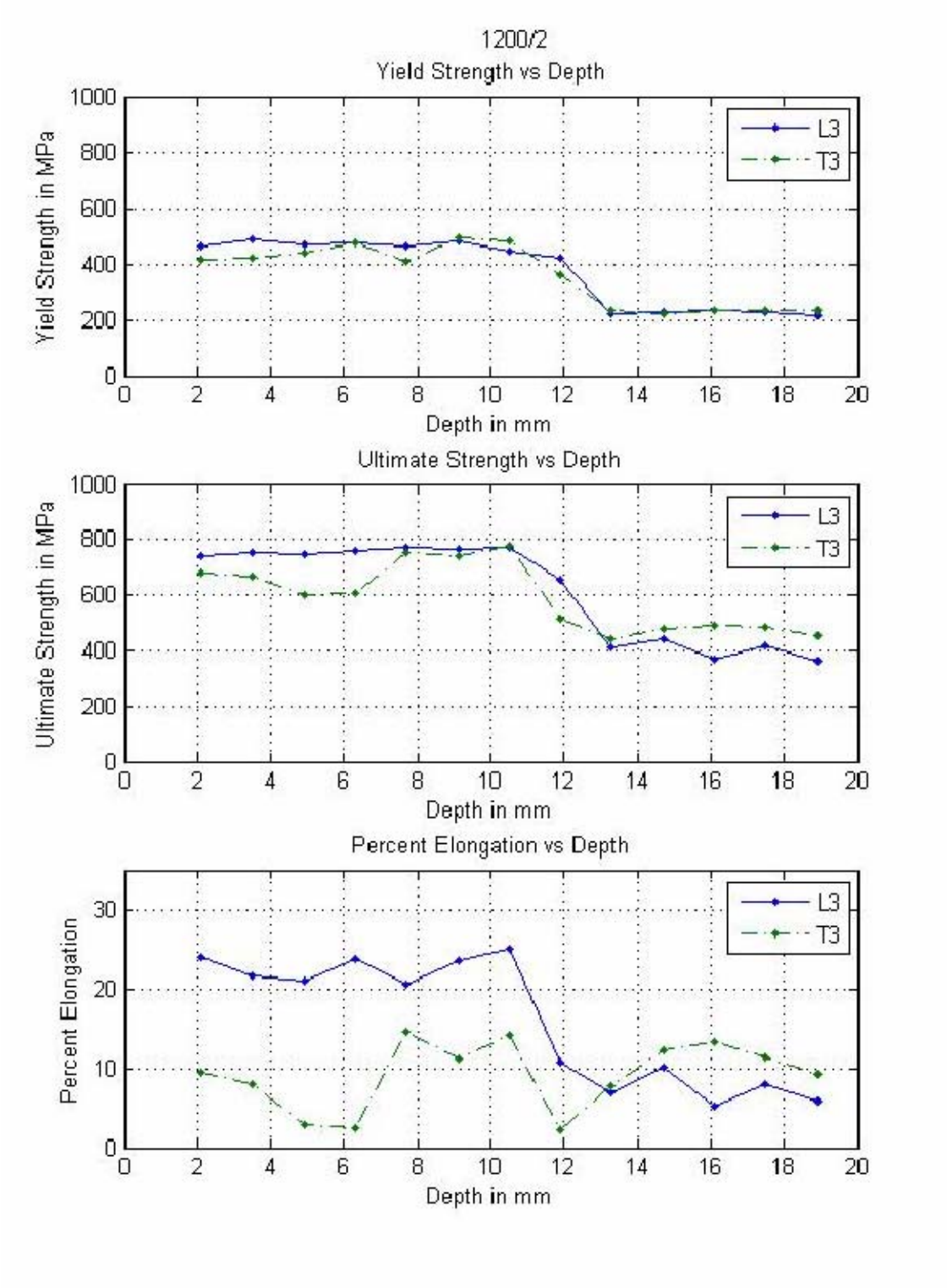

Figure 22. Material Properties vs. Depth in Tensile Blocks L3 & T3, for 1200/2 plate.

C. FRACTOGRAPHY

To gain a better understanding of fracture mechanisms, thirty two tensile samples were selected from these tests and examined in the SEM by secondary imaging methods. These included high strength/high ductility samples, base plate samples, samples near the TMAZ, and those that displayed low ductility in regions where high ductility was anticipated. Altogether, 168 SEM images were obtained for the following specimens: 800/4{L1(b, c, d), L2(i, j, k), T2 (c, j, n)}; 1000/3 {L1(d, e, f, g)};1200/2 {L2 (d, j, m), T1(d, e, i, j), T2(d, e, f, g), T3(c, d, e, f)}; and four base-metal samples. The underlined samples had lower than anticipated ductility values. Representative results from the samples will be included in this summary.

Figures 23 and 24 compare base metal and stir zone fractography. Figure 23 shows two SEM fractographs taken at 200x and 400x magnification of tensile sample 1200/2-L2-m which was located in base metal, showing that fracture is a combination of ductile and brittle modes. The surface exhibits microvoid formation and coalescence, as well as cleavage cracking. This sample had 11% ductility. It is likely that failure occurs by microvoid formation and coalescence in the primary α phase while cleavage cracking occurs in the eutectoid constituents.

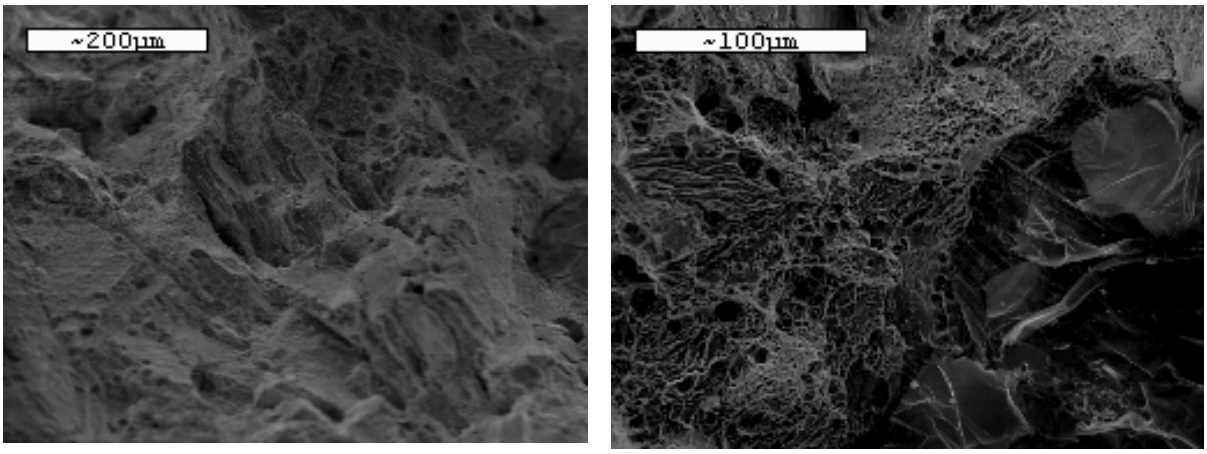

Figure 23. SEM of 1200/2-L2-m, 200x and 400x magnification.

Figure 24 shows two SEM photos taken at 200x and 400x magnification of tensile sample 1200/2-L2-d. This sample includes only stir zone material in its gauge length and had fine, equiaxed α grains in the microstructure. These fractographs only exhibit

microvoid formation and coalescence features. The sample was very ductile; it had 28% elongation. The stir zone fractography results all showed similar fracture mechanics as indicated in Figure 24.

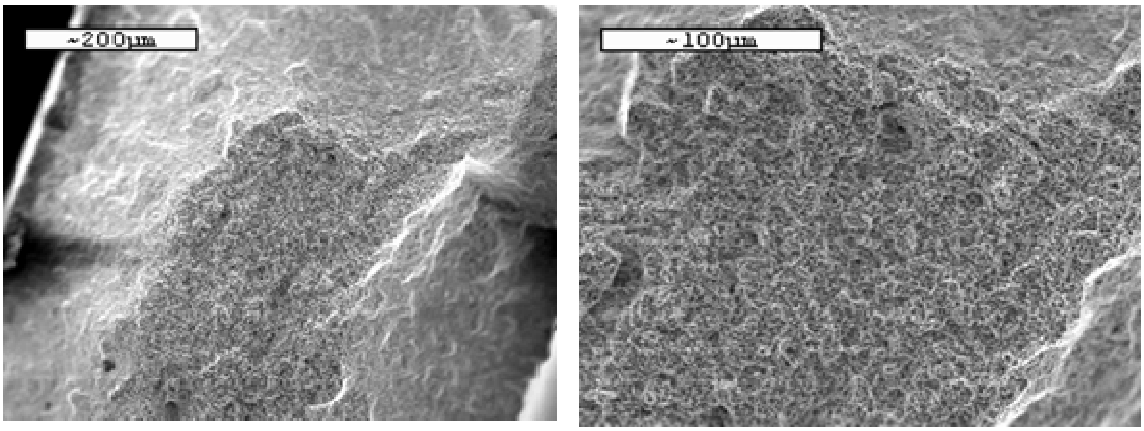

Figure 24. SEM of 1200/2-L2-d, 200x and 400x magnification.

The TMAZ/HAZ zone is of particular significance. Within a small volume of material the material properties decline significantly, sometimes to values equal with or slightly less than the base metal properties. Figure 25 contains fractographs at 200x magnification showing both ductile and brittle modes of fracture. Photos are from the 1200/2-L2-j tensile specimen which had 8.4% ductility.

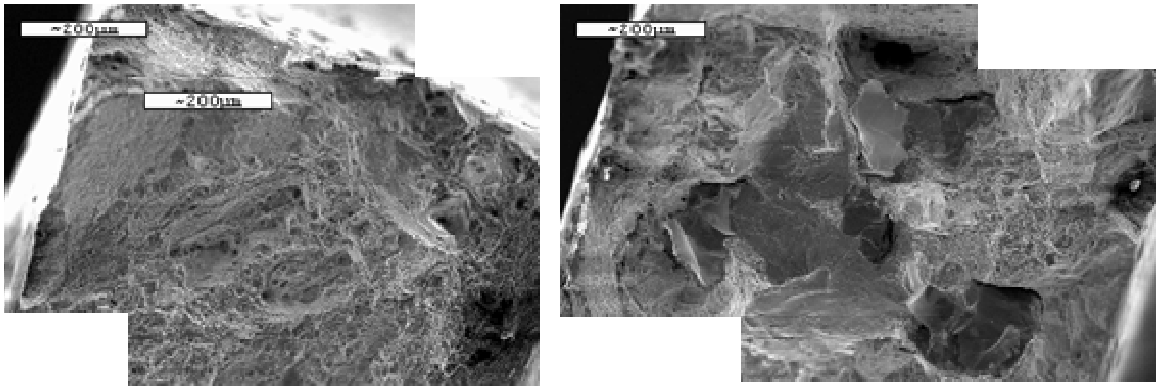

Figure 25. SEM of 1200/2-L2-j, 200x magnification.

Figure 26 shows the same tensile sample but at a higher magnification of 400x. At this higher magnification, significant details of the fracture surfaces become apparent. Regions of microvoid formation and coalescence surround large features that indicate cleavage cracking. These later features may exceed 100 µm in extent and present a

faceted appearance. These features are likely the dark-etching constituent observed in the TMAZ/HAZ surrounding the stir zone.

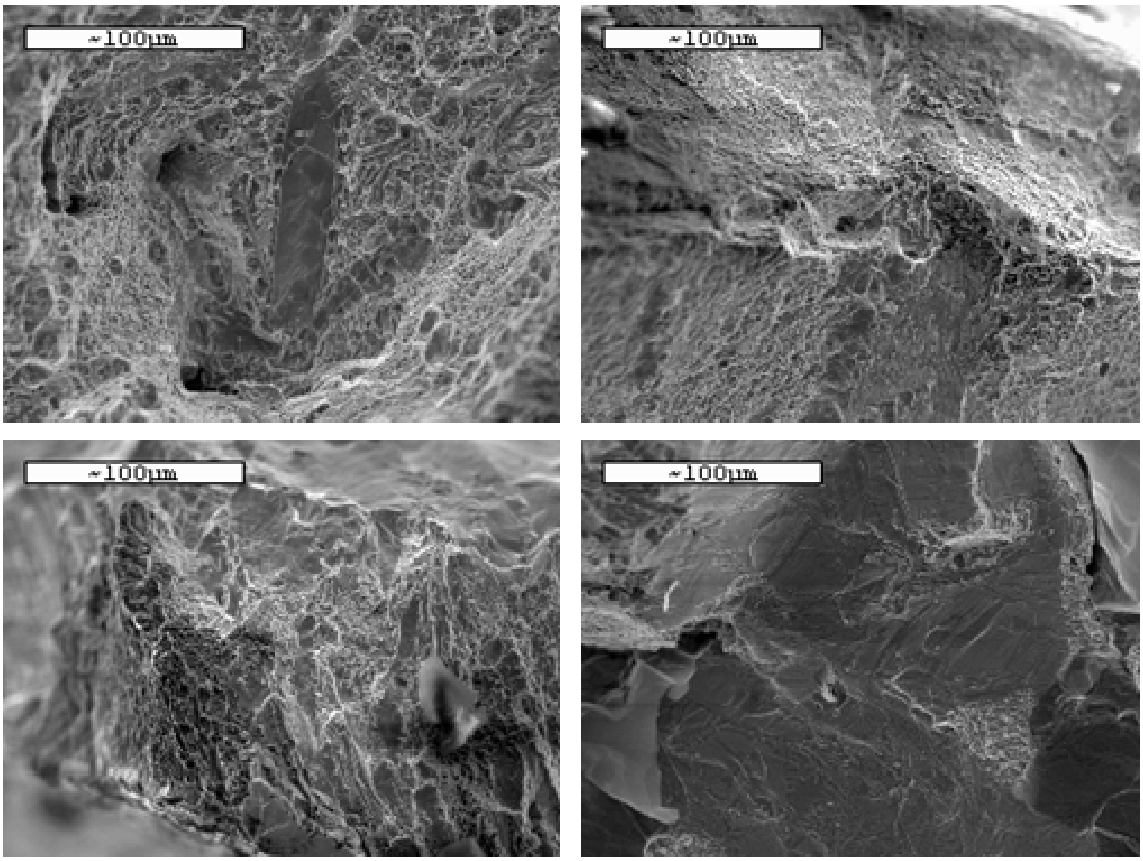

Figure 26. SEM of 1200/2-L2-j, 400x magnification.

Figure 27 shows tensile specimen 800/4-L2-i which is just above the TMAZ/HAZ interface. This sample displayed a ductility of 27%. Figure 28 is tensile sample 800/4-L2-j which is just after the TMAZ/HAZ interface. This sample displayed a ductility of 6%. Note how the fracture mechanism is primarily microvoid formation and coalescence in Figure 27, and that it becomes, again, a mixture of competing mechanisms in Figure 28. The images in Figure 28 are arranged to show the spatial relationship among the three photos and indicate cleavage cracking appears to have occurred at the corners of this tensile specimen. In general, tensile samples from the TMAZ/HAZ locations below the stir zone exhibited mixed fracture modes. Again, cleavage cracking likely reflects low energy fracture of the dark-etching martensitic constituent in these locations.

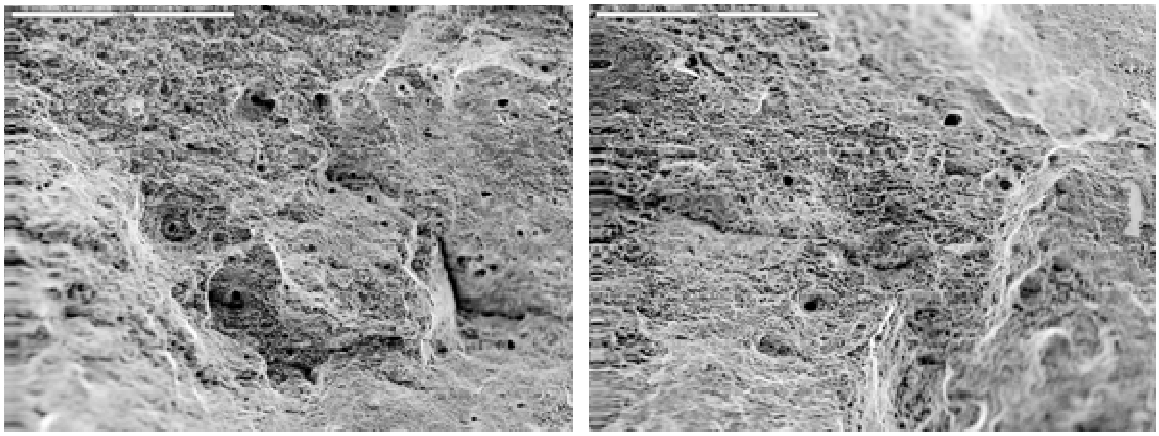

Figure 27. SEM of 800/4_L2-i sample, 200x magnification.

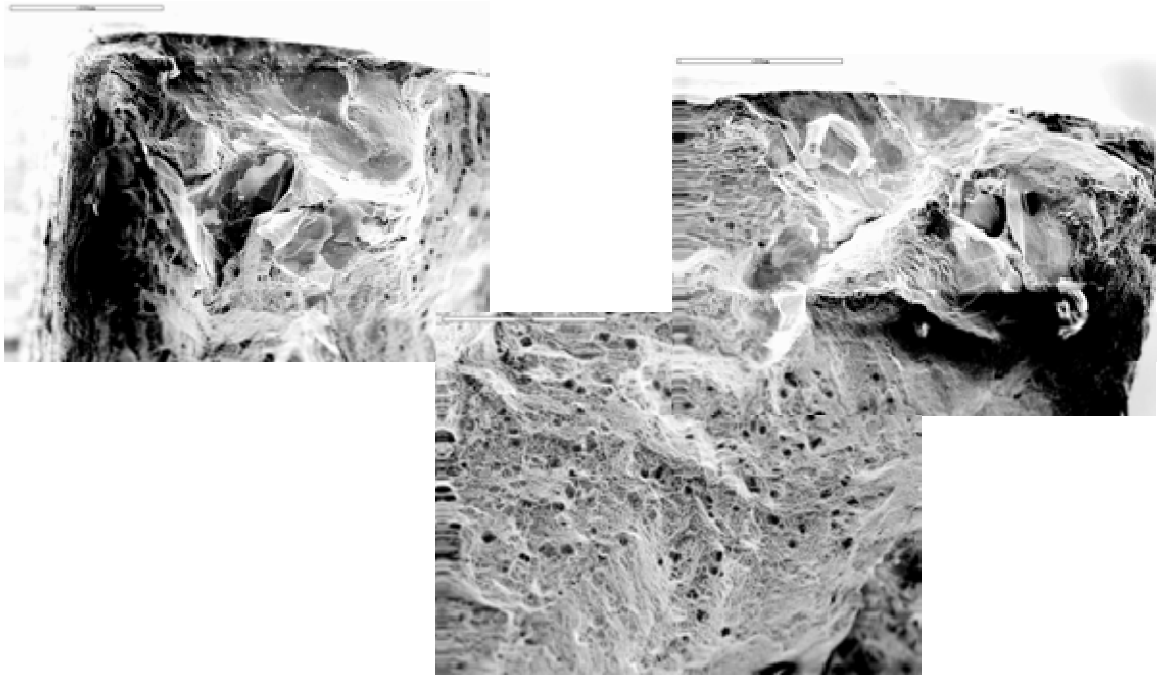

Figure 28. SEM of 800/4-L2-j sample, 200x magnification.

Low ductility samples within the stir zone were also examined. In the Figure 29, the tensile specimen should have exhibited a ductility value around 25% (based on its neighbors), but the actual value observed was 13.6%. The dark areas are the likely cause of the low ductility. The tensile samples before and after this particular specimen did not have these observed dark areas; their fractographs displayed microvoid formation and coalescence. These dark-appearing regions may be voids or other processing-induced defects, or inclusions in the original casting that were incompletely broken up and redistributed.

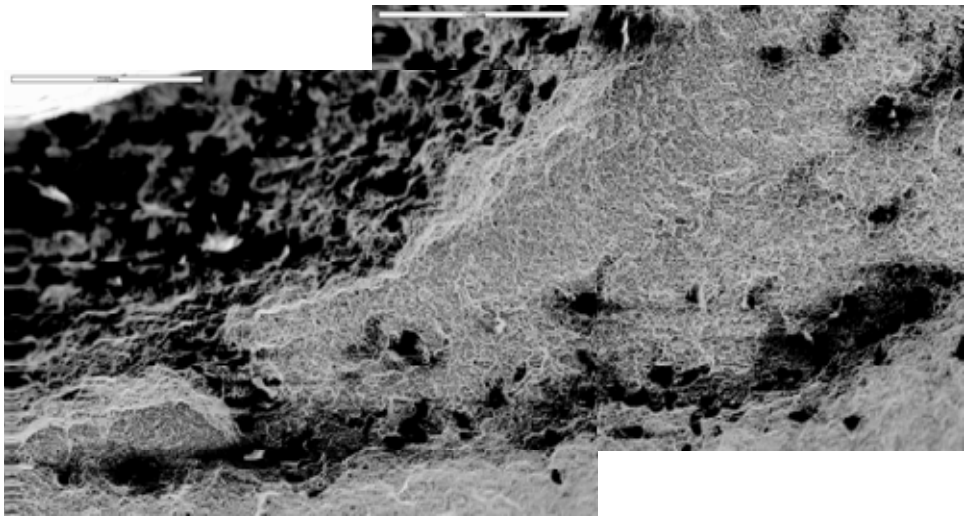

Figure 29. SEM of 1000/3-L1-f sample, 200x magnification.

SEM data from the transition in the T1 region yielded noteworthy results. Figure 30 is from tensile sample 1200/2-T1-e, the first sample to display low ductility (4%) in the T1 tensile blank. It clearly shows brittle fracture mechanisms as well as some microvoids.

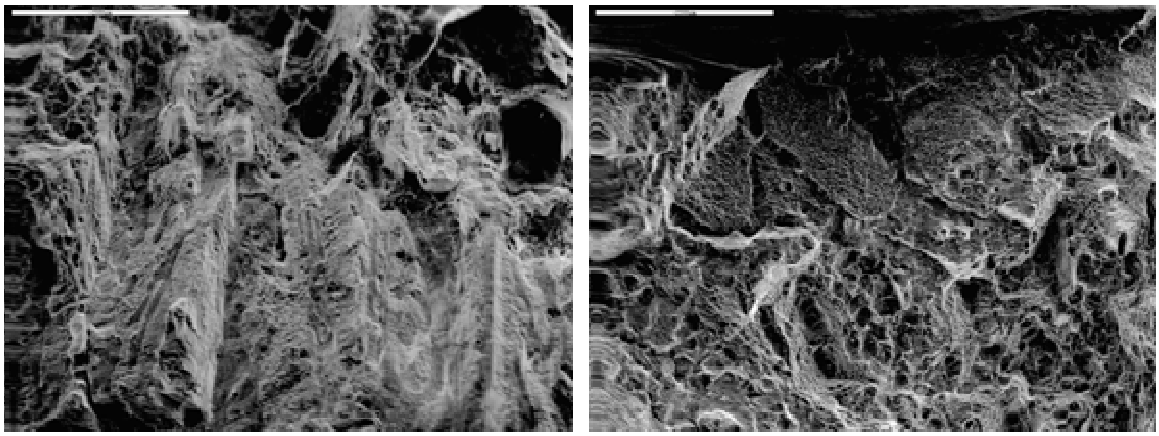

Figure 30. SEM of 1200/2-T1-e sample, 200x magnification.

Figure 31 shows the same samples but at 400x magnification. This clearly shows a cleavage fracture. Optical microscopy likely will indicate that such cleavage cracking reflects the presence of a martensitic constituent in this region. This would indicate that high cooling rates in the initial traverse resulted in this feature, and that process modifications to reduce these rates may be beneficial.

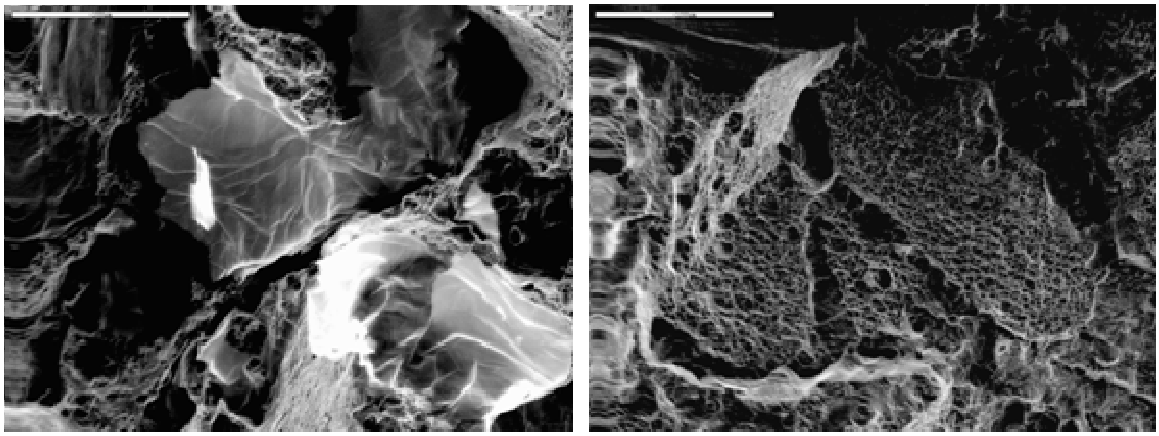

Figure 31. SEM of 1200/2-T1-e sample, 400x magnification.

Figures 32 and 33 show samples 1200/2-T3-c and 1200/2-T3-d. These samples exhibited ductility values of 8%, and 3%, respectively. In both cases, the fracture surface exhibit distinct step-like features suggesting failure at bands that may arise at locations where the second pass overlaps the first. The initial advancing side interface may not have been broken up and dispersed.

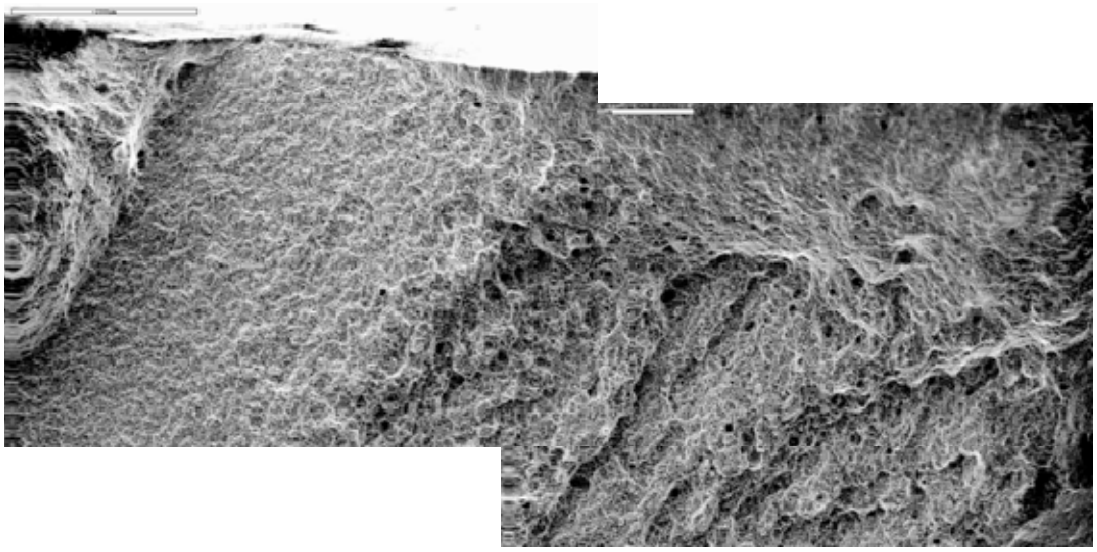

Figure 32. SEM of 1200/2-T3-c sample, 200x magnification.

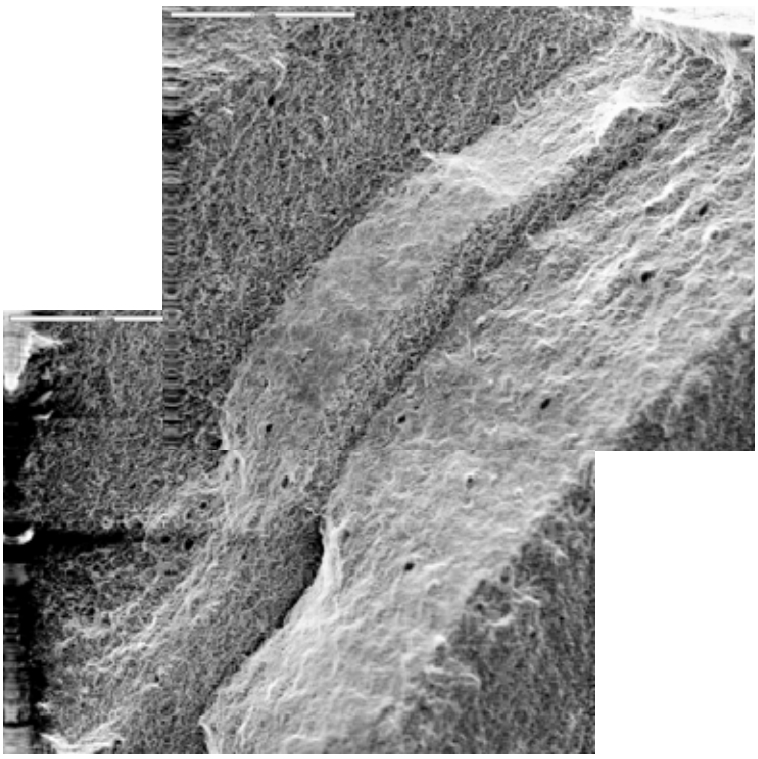

Figure 33. SEM of 1200/2-T3-d sample, 200x magnification.

D. COMPARISON WITH FUSION WELDING

A final point of comparison is how the plates processed by FSP compare with similar NAB material which has been fusion welded. The goal of this FSP research is to reduce or eliminate conventional fusion welding to repair porosity during the post-processing of cast NAB propellers. Figure 34 is a plot comparing the data generated in this report with previous research results for a six-pass Gas Metal Arc Weld (GMAW) overlay in similar NAB material. Welding involved the following parameters: 24.5 V, 239 Amps, and 8.5 IPM, and used Ampcotrode 46 electrode wire as the filler [10, 12]. The depth of the weld metal was greater than the stir zone depth and, so, the data has been normalized to the depth of the process zones for these different processes. A depth of one (1) indicates either the stir zone or fusion zone boundary with the heat affected base metal. Both FSP data and fusion welding data were taken from tensile samples oriented in the longitudinal direction with respect to tool/arc travel.

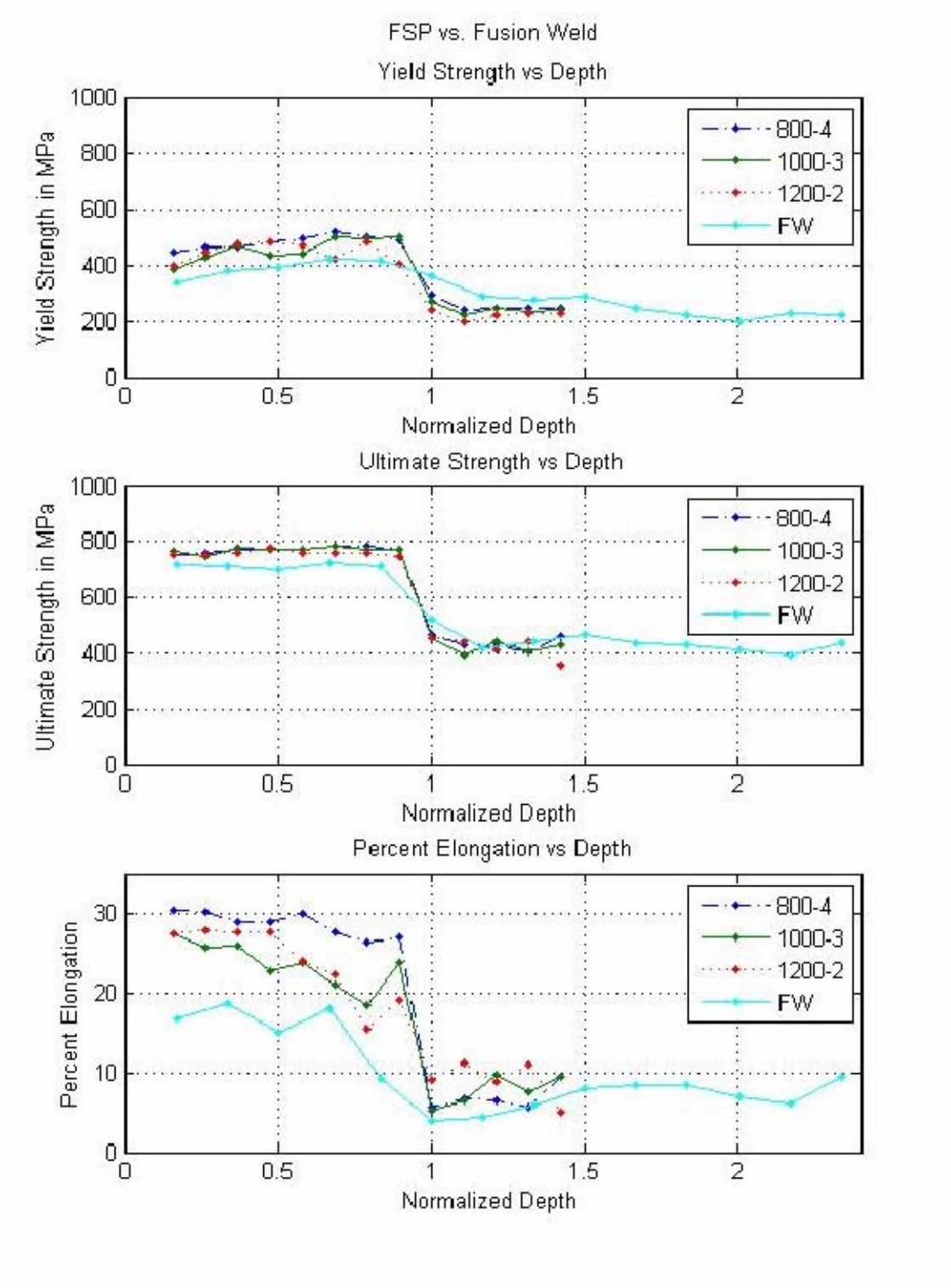

Figure 34. Normalized Plot Comparing Material Properties of FSP verse Fusion Welding. After [10].

The FSP material has consistently higher values in all three material properties than the fusion welded material. Both experience sharp declines with respect to their material properties as they pass from their processed zones into the TMAZ or HAZ. The FSP material however does not exhibit any values of ductility less than the fusion welded material. These results suggest that FSP is an appropriate substitute or replacement for fusion welding on NAB material. Additionally, since the loss of ductility in the region between the process zone and base metal (i.e., the TMAZ or HAZ) occurs in both processes, the ductility loss phenomenon is a thermo effect and not a thermomechanical effect.

THIS PAGE INTENTIONALLY LEFT BLANK

V. CONCLUSIONS AND RECOMMENDATIONS

A. CONCLUSIONS

1. The rectangular spiral pattern provided essentially uniform material properties, including ductility, within the region of overlapping passes.
2. High ductility reflected the presence of fine α grains and fine β transformation products.
3. Areas of low ductility were at the stir zone/TMAZ/HAZ interface as well as near the first pass. Conventional fusion welding experiences the same loss of ductility in similar regions. This suggests that the lose of ductility with FSP material is a thermal effect and not a thermomechanical effect.
4. FSP provides better material properties within the stir zone and no worse in the SZ/TMAZ/HAZ interface than fusion welding.
5. Friction Stir Processing may replace conventional fusion weld repair in NAB material propeller post-processing and similar engineering applications.

B. RECOMMENDATIONS FOR FUTURE RESEARCH

The following are suggestions for future research:

1. Conduct additional testing of mechanical property data within the first pass interface (T3 region) of the rectangular spiral patterns studied in this research.
2. Identify whether the loss of ductility occurs in the stir zone/TMAZ interface or the HAZ region using smaller tensile samples.
3. Preheating of the material prior to the first pass of the rectangular spiral pattern may reduce the loss of ductility found in T3 specimens.
4. Design the rectangular spiral pattern to reprocess the first pass immediately after completing the second pass but prior to entering the spiral pattern.

THIS PAGE INTENTIONALLY LEFT BLANK

LIST OF REFERENCES

1. Mishra, R.S., Ma, Z.Y., "Friction Stir Welding and Processing," *Materials Science and Engineering*, v. 50, p. 1-78, 2005.

2. Thomas, W.M., et al., "Friction Stir Butt Welding", International Patent Appl. No. PCT/GB92/02203 and GB Patent Appl. No. 9125978.8, Dec 1991, U.S. Patent No. 5,460,317 – from [15] in support of information by Stephan Kallee and David Nicholas, TWI.

3. Oh-Ishi, K. and McNelley, T., "The Influence of Friction Stir Processing Parameters on Microstructure of As-Cast NiAl Bronze*" Metallurgical and Materials Transactions, v.* 36A, p. 1575-1585, 2005.

4. Mahoney, Murray W., Bingel, William H., Mishra, Rajiv S., *Materials Science Forum*, v. 426-432, p. 2843-2848, 2003.

5. Mishra, R. S. and Mahoney, M. W., "Friction Stir Processing: A New Grain Refinement Technique to Achieve High Strain Rate Superplasticity in Commercial Alloys," *Materials Science Forum*, v. 357-359, p.507-514, 2001.

6. Culpan, E. A. and Rose, G., "Microstructural Characterization of Cast Nickel Aluminum Bronze," *Journal of Materials Science*, v. 13, p. 1647-1657, 1978.

7. Hasan, F., Jahanafrooz, A., Lorimer, G.W., Ridley, N., "The Morphology, Crystallography, and Chemistry of Phases in As-Cast Nickel-Aluminum Bronze," *Met. Trans A*, v.13a, p.1337-1345, 1982.

8. Wenschot, P., "The Properties of Ni-Al Bronze Sand Cast Ship Propellers in Relation to Section Thickness," *International Shipbuilding Progress*, v. 34, p.112-123, 1987.

9. Williams, Robert A., MS Thesis, "A Microstructural and Mechanical Property Correlation of Friction Stir Processed Nickel Aluminum Bronze" Naval Postgraduate School, Monterey, CA, Sep 2004.

10. Fuller, Michael D., MS Thesis, "Friction Stir Processing and Fusion Welding in Nickel Aluminum Propeller Bronze" Naval Postgraduate School, Monterey, CA, Mar 2006.

11. J amison, Jay D., MS Thesis, "Modeling of Thermal and Mechanical Effects During Friction Stir Processing of Nickel-Aluminum Bronze" Naval Postgraduate School, Monterey, CA, Sep 2004.

12. Murray, David L., MS Thesis, "Friction Stir Processing of Nickel-Aluminum Propeller Bronze in Comparison to Fusion Welds" Naval Postgraduate School, Monterey, CA, Sep 2004.

13. Pierce, F. A., MS Thesis, "The Isothermal Deformation of Nickel-Aluminum Bronze in Relation to the Friction Stir Processing," Naval Postgraduate School, Monterey, CA, Jun 2004.

14. Mishra, R.S., *Advanced Materials and Processes*, v. 161(10), p. 43-46, 2003.

15. Mishra, R.S., Ma, Z.Y., and Charit, I., *Mater. Sci. Engineering A*, v. A341, p. 30710, 2003.

16. Ma. Z.Y., Mishra, R.S., and Mahoney, M.W., "Friction Stir Welding and Processing II", TMS, Warrendale, PA, p. 221-230, 2003.

17. Sahoo, M., "Structure and Mechanical Properties of Slow-Cooled Nickel-Aluminum Bronze Alloy C95800," *AFS Trans*, v. 90, p. 913-926, 1982.

18. Culpan, E.A. and Rose, G., "Corrosion Behavior of Cast Nickel Aluminum Bronze in Sea Water," *British Corrosion Journal*, v. 14, 160-166, 1979.

19. American Society for Testing and Materials (ASTM) B148-93a, Standard Specification for Aluminum-Bronze Sand Castings.

20. Ohishi, K., McNelley, T.R., "The Influence of Friction Stir Processing Parameters on Microstructure of As-Cast NiAl Bronze," *Metallurgical and Materials Transactions*, v.36a, p.1575-1585, 2005.

21. Hasan, F., Lorimer, G.W., Ridley, N., "Crystallography of Martensite in a Cu-10Al-5Ni-5Fe alloy," Journal de Physique, v.43, p.C4 653-C4 658, 1982.

22. Mahoney, M. W., Rockwell Scientific Corporation, private communication, February 2005.

23. Ohishi, K., McNelley, T.R., "Microstructural Modification of As-Cast NiAl Bronze Friction Stir Processing," *Metallurgical and Materials Transactions*, v.35a, p.2951-2960, September 2004.

24. American Society for Testing and Materials (ASTM) E-8, Standard Test Methods for Tension Testing of Metallic Materials.

INITIAL DISTRIBUTION LIST

1. Defense Technical Information Center
   Ft. Belvoir, Virginia

2. Dudley Knox Library
   Naval Postgraduate School
   Monterey, California

3. Dr. Terry R. McNelley
   Department of Mechanical and Astronautical Engineering
   Naval Postgraduate School, Monterey, CA

4. Dr. Anthony J. Healy
   Department of Mechanical and Astronautical Engineering
   Naval Postgraduate School, Monterey, CA

5. William Palko
   Naval Surface Warfare Center (NSWC) Carderock Division
   Bethesda, MD

6. Murray W. Mahoney
   Teledyne Scientific Corporation
   Thousand Oaks, CA